Selective Heavy Element Sensing with a Simple Host:Guest Fluorescent Array

Yang Liu,[2] Magi Mettry,[1] Adam D. Gill,[3] Lizeth Perez,[1] Wenwan Zhong[1, 2*] and Richard J. Hooley[1,3*]

[1]Department of Chemistry; [2]Environmental Toxicology Program; [3]Department of Biochemistry and Molecular Biology; University of California-Riverside, Riverside, CA 92521, U.S.A. E-mail: richard.hooley@ucr.edu; wenwan.zhong@ucr.edu, Fax: +1 951 827 4713.

ABSTRACT: A simple three component array of host:fluorophore complexes is capable of sensitive and selective discrimination of heavy metal ions, including lanthanide and actinide salts in aqueous solution. Instead of applying optical sensors that only use "single-mode" detection, i.e. coordination of the metal to a specific ligand and monitoring the change in emission of an appended fluorophore, we exploit a series of host:fluorophore complexes that are affected by the presence of small amounts of metal ions in aqueous solution in different ways. Variable host:metal and host:guest:metal interactions lead to both turn-on and turn-off fluorescence sensing mechanisms, enhancing the discriminatory properties of the array. The limit of detection for certain metals is as low as 70 nM, and highly similar metals such as lanthanides and actinides can be easily distinguished at low micromolar concentrations in complex salt mixtures.

Introduction

Heavy metals such as chromium, lead, and mercury pose a persistent risk to ecosystems, [1] and are also a threat to human health, causing severe issues such as memory loss, learning deficits, blindness and deafness, kidney damage and cancers.[2,3] In addition, employment of rare earth (RE) metals including lanthanides and actinides in industry has been increasing. These elements can cause mutations and cancers, and radioactivity imposes acute danger to human beings and ecosystems. Therefore, it is of paramount importance to sensitively and selectively monitor toxic heavy and RE metal contents in the environment.[4,5] The challenge in monitoring heavy metal pollutants lies in the complexity of environmental samples, and calls for simple survey techniques that can detect multiple metals selectively and sensitively, in a fast and high-throughput manner. [6,7] The most selective probes for metal ions are DNA-based, and can be employed in fluorescence-based assays for sensitive metal detection.[8-17] However, few are found for RE metals[8,9,15,16] and they are rarely applied to monitor complex metal mixtures, due to their synthetic complexity and cost. Electrochemical sensors have been developed for heavy or RE metals, but display relatively poor sensitivity and selectivity.[18,19] Small molecule metal sensors are attractive due to their simplicity and scalability,[20,21] but can be limited in their selectivity. Selective discrimination between ions that have extremely similar charges, electron configurations and coordination geometries is challenging. Whereas transition metals display varying coordination geometries and numbers, the coordination chemistry of the RE metals is quite consistent across the series, with the largest differences being in effective ionic radius (EIR) and charge:size ratio. Those differences are small: La^{3+} and Yb^{3+} are only separated by 0.2 Å in size, and adjacent rare earths are exceptionally similar in EIR.[22,23] As a result, the RE metals are challenging targets for selective optical sensing by small molecule systems, especially at low concentrations. For example, while the concentration of uranyl ion in seawater is only 3 ppb,[24] contaminated waste streams in rivers can contain as high as 11.5 ppm,[25] and sensors that can function in that range are highly applicable for environmental remediation.[26]

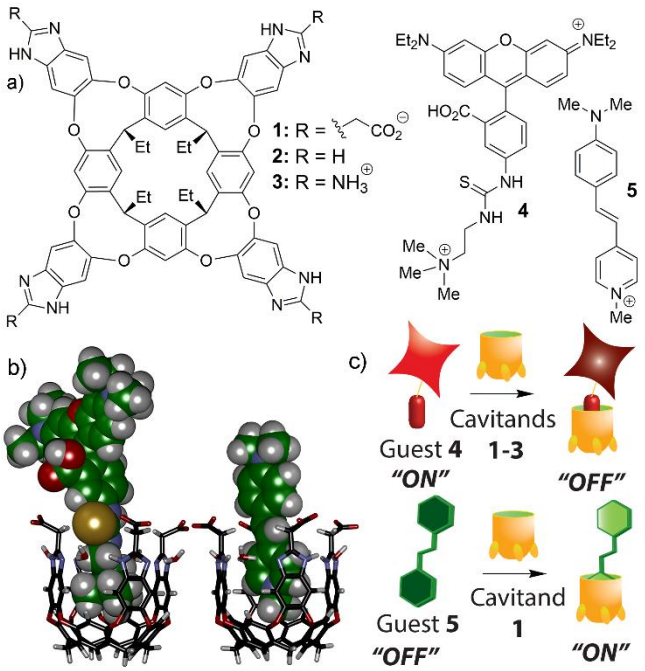

Figure 1. a) Structure of hosts **1**-**3**, guests **4** and **5**; b) minimized models of the **1**•**4** and **1**•**5** host:guest complexes (SPARTAN); c) Illustration of the turn-on and turn-off fluorescence detection processes.

One method to increase the sensitivity of optical sensors is to combine multiple detectors into a sensor array.[27-33] Each array element can respond to several metals and a number of such elements are combined to yield a signal pattern from all the metals in the sample. The patterns from all array elements can be treated by discriminant analysis[34,35] to extract the quantitative information about the analytes and selectively recognize the presence of multiple metals in the mixture. While some arrayed optical sensors for heavy metals are

known,[30] selective discrimination of highly similar metals is challenging, and analysis of RE metals via these techniques is limited. Even with arrayed sensors, the strategy of combining a metal coordinator and a covalently appended fluorophore for "turn-off" sensing is limited by the selectivity of metal ion coordination.

Here we offer an alternative strategy: instead of applying optical sensors that only use "single-mode" detection, i.e. coordination of the metal to a specific ligand, and monitoring the change in emission of an appended fluorophore, one can exploit a series of host:fluorophore complexes that are affected by the presence of small amounts of metal ions in aqueous solution in different ways. The sensing candidates are shown in Figure 1: the hosts are water-soluble deep cavitands, molecules that display a defined cavity capable of binding suitably sized and charged species in aqueous solution.[36-41] By varying the charge and H-bonding abilities at the upper rim while maintaining the internal cavity, selective host:guest interactions can be enhanced, and pH-responsive recognition is possible.[42,43] The molecular recognition properties of cavitands **1**-**3** are affected by numerous factors, including salt concentration and type, pH, and the presence of surfactants. These subtle changes in environment can alter the binding affinity of fluorescent guests in the hosts, giving a simple optical readout of affinity changes. By combining variably functionalized hosts with different fluorescent guests at varying pH in an arrayed format, a "chemical nose" sensor[44-49] can be created that is capable of highly selective discrimination of similar ionic species at micromolar concentration in buffered water.

The sensing applications performed to date have involved detecting species that bind inside the host cavity and displace the target fluorophore, such as post-translationally modified peptides.[42] The sensitivity of the system to environmental variations suggested that other interactions could be exploited for detection. The multiple carboxylate groups in **1** are in close proximity to each other, and are easily capable of free rotation to chelate a metal ion, allowing effective binding, even in aqueous solution. Here we show that a simple array of host:fluorophore complexes is capable of selective sensing and discrimination of highly similar heavy metal ions, including lanthanide and actinide salts in aqueous solution, via multiple fluorescence enhancement and quenching mechanisms.

Experimental Section

General. Cavitands **1**,[36] **2**,[50] **3**[51] and guest **4**[43] were synthesized according to literature procedures. DSMI **5** (trans-4-[4-(Dimethylamino)styryl]-1-methylpyridinium iodide) was purchased from Sigma-Aldrich (St. Louis, MO) and used without further purification.All the metal salts were purchased from Sigma-Aldrich (St. Louis, MO) and Alfa Aesar (Tewksbury, MA), and they were directly used without further purification. The heavy metal ions were produced from their respective chloride salts as following with several exceptions: $MgCl_2$, $CaCl_2$, $MnCl_2$, $FeCl_2$, $CoCl_2$, $NiCl_2$, $CuCl_2$, $ZnCl_2$, $CdCl_2$, $Hg(OAc)_2$, $Pb(NO_3)_2$, $LaCl_3$, $CeCl_3$, $ErCl_3$, $ThCl_4$ and $UO_2(OAc)_2$. Molecular modeling (semi-empirical calculations) was performed using the AM1 force field using SPARTAN.

Experimental Procedures

Fluorescence sensor array with metals. In general, the fluorescence assay was carried out by mixing 10 μL of guest **4** (30 μM) or guest **5** (15 μM), 10 μL of the cavitand (40 μM for **1**•**4** or 200 μM for **1**•**5**, 50 μM for **2**•**4** or **3**•**4**), 70 μL of the incubation buffer (Tris pH 7.4 or Bis-Tris pH 5.5) in a 96-well plate, adding 10 μL of different metal salt solution to bring the total volume up to 100 μL, and incubating with mild shaking for 15 mins at room temperature. The fluorescence signal (F) was recorded in a Perkin Elmer Wallac 1420 Victor 2 Microplate Reader (PerkinElmer) with the Ex/Em wavelengths at 530/605 nm for guest **4** or 485/605 for guest **5**.

Real sample detection. Tap water and environmental lake water were collected and used without further treatment. For tap water spike, metal stock solutions (Pb^{2+} and UO_2^{2+}) were first prepared in DI water with a concentration of 1 mM and then spiked into tap water sample with a final concentration of 20 μM. Other salts were also prepared and added the same way with a final concentration of 20 μM respectively. The as-prepared tap water sample was then added into the sensor array. After 10 minutes incubation, fluorescence was read by the plate reader and analyzed with LDA. For environmental lake water tests, mixtures of Th^{4+} and La^{3+} were prepared with different ratios, varying from 0:21 to 21:0 in 3 μM increments. The analysis procedures were identical to those used for the tap water samples. Samples A, B and C were also prepared the same way and then tested by ICP-AES.

SELDI TOF-MS. Graphene oxide stock solution in water was first diluted to 1 mg/mL in either Tris buffer (pH 7.4, 20 mM) or Bis-Tris buffer (pH 5.5, 20 mM). Metal (100 μM) and cavitand **1** (10 μM) were mixed and incubated for 15 minutes in the same buffer condition. After incubation, 1 μL of above metal and cavitand mixture was mixed with graphene oxide and spotted on a stainless steel Opti-TOF™ 96 targets plate, and allowed to dry completely before introducing into the mass spectrometer. Analysis was carried out on an AB Sciex 5800 TOF/TOF proteomics analyzer with a laser irradiation at a repetition frequency of 1,000 Hz. A laser intensity index of 2900 was used for sample ionization and the MS spectra were acquired in the negative reflector mode within the mass range from 100 to 2,000 Da. The SELDI analysis of cavitand **1**, fluorescent guest (either **4** or **5**) and metal was also performed via this method. The final concentration of cavitand **1**, guest and metal was 10 μM, 7.5 μM and 100 μM respectively.

K_d calculations. The calibration curves of fluorescence response vs. metal concentration were obtained by adding 0 – 100 μM of metal into the sensor solution that contained either **4**•**1** ([**1**] = 4 μM, [**4**] = 3 μM) in PH 7.4 or pH 5.5 buffer, and **5**•**1** ([**1**] = 20 μM, [**5**] = 1.5 μM, pH 7.4). The fluorescence was recorded after 15 mins of mixing in the plate reader as described above.

In the metal-cavitand-guest complex formation model,[52] the curves were fitted with the Hill equation using Origin Pro 8.0 shown below:

$$\frac{F}{F_{max}} = \frac{F_{start}}{F_{max}} + \left(\frac{F_{end}}{F_{max}} - \frac{F_{start}}{F_{max}}\right)\frac{[metal]^n}{k^n + [metal]^n} \qquad (1)$$

$$K_d^{MC} = k^n$$

where F is the fluorescence reading, F_{start} is starting fluorescence, F_{end} is the ending plateau fluorescence, $[metal]$ is the metal concentration, k is the microscopic dissociation constant, and n is the binding cooperativity. K_d^{MC} is the apparent dissociation constant, representing the stability of metal binding to the cavitand-guest sensor complex.

In the displacement model, K_d^D, the dissociation constant for the metal-cavitand complex were calculated following the typical approach for determination of inhibitor binding constant in protein-ligand-inhibitor binding assays.[20] The titration curves were fitted to the exponential decay equation and obtain the constant t1:

$$F/F_{max} = A\, e^{-[metal]/t_1} \qquad (2)$$

Then IC50 was calculated from t_1 using the equation of $IC_{50} = \ln(1/2)\, t_1$. Followed, K_d^D was obtained by the following equation:

$$K_d^D = IC_{50}/(\frac{[L]_{50}}{K_d} + \frac{[cavitand]_0}{K_d} + 1) \qquad (3)$$

where $[L]_{50}$ is the concentration of the free metal ions at 50% inhibition (approximated to be the starting small molecule concentration), $[cavitand]_0$ is the cavitand concentration at 0% inhibition, and K_d is the dissociation constant for the cavitand **1**•**4** or **1**•**5** complex.[43]

Data analysis. Linear Discriminant Analysis (LDA), Jackknife validation and Hierarchical clustering analysis (HCA) were completed with RStudio (Version 1.0.136), an integrated development environment (IDE) for R (version 3.3.2). Fluorescence data was first stored as an excel file, and then read into a matrix in RStudio. The internal function "princomp()" was used to perform PCA; the 'lda()' function was called for Jackknife Validation with the "CV" set as "true". One replicate was left out of the training set, and the LDA classifier was fitted on the input data. The output was recorded in a two-dimensional table. HCA was performed with two steps: the Euclidean distance between any two objects within the dataset was first calculated and recorded into a two-dimensional matrix; then the matrix was used as the input for the built-in HCA function "hclust()", and the result was drawn with the "plot()" function. Confidence ellipses were drawn with the data obtained from PCA using Matlab (version R2016b) and a self-developed script. The full Matlab script is available upon request. The 3D scatter plot was performed with Plotly's R package version 4.

Results and Discussion

We investigated two reporter molecules: RhB guest **4**, which contains a trimethylammonium (R-Me_3^+) group for binding in hosts **1**-**3**, and dimethylaminostyrylmethylpyridinium iodide (DSMI) **5**. Guest **4** displays the fluorescent Rhodamine B group above the cavity of the hosts, and strong intermolecular fluorescence quenching is observed via photoinduced electron transfer.[43] The affinity of **4** for cavitands **1**-**3** varies from 2.8 μM (**2**, pH 3.3) to 190 nM (**3**, pH 9.0), and >98% quenching of the fluorescence of **4** is observed upon binding. DSMI **5** has a size, shape and charge profile that suggest it would be an excellent guest for **1**-**3** in water, and it is well-known to display enhanced fluorescence upon binding in hydrophobic environments, such as the cavity of host molecules hexasulfonatocalix[6]arene[53,54] or cucurbit[7]uril.[55] Interestingly, DSMI **5** behaves quite differently to RhB guest **4**: upon its binding to anionic cavitand **1**, a strong *enhancement* in fluorescence of **5** is observed. The maximal fluorescence increase is over 30-fold at pH 3.3, which is far larger than the observed increase seen when bound in CX6[53] or CB7 (Figure S-1, Supporting Information).[55] The enhancement is pH dependent: the maximum increase was close to 20-fold at pH 5.0 and 7.4, while at pH 9.0 less than 5-fold increase was observed (72.6 μM **1**, 1.5 μM **5**, 100 mM phosphate or carbonate buffer adjusted to the corresponding pH, see Figure S-2). The excitation and emission occurred at λ = 485 nm and 605 nm, respectively, and the combination of 1.5 μM DSMI **5** with 20 μM of cavitand **1** were chosen as the optimal sensing conditions (Figures S-3 & S-4). The dissociation constant K_d (**5**•**1**) was found to be 23.1 μM through non-linear regression analysis of the fluorescence enhancement curve at pH 7.4 (Figure S-5), an order of magnitude lower than that of **4**•**1**. The lower affinity of **5** necessitated the use of an excess of **1** to reach saturation in fluorescence change for sensing purposes (Figure S-4). The **5**•**1** complex was quite stable and the fluorescence was not affected by the presence of liposomes (see Figure S-6). Interestingly, the fluorescence of DSMI **5** was not significantly enhanced by cavitands **2** or **3** in aqueous solution, suggesting that both shape and charge-based complementary interactions are required for strong binding between DSMI **5** and cavitand **1**. The lower solubility of **2** and **3** prevents sufficient cavitand being present to bind a significant proportion of 5 in solution at the concentrations used.

The individual host:guest combinations were exposed to micromolar concentrations of a series of heavy metal salts in buffered aqueous solution. Tris and Bis-Tris buffers (20 mM) were used to minimize the presence of competitive ions in the system, and focus solely on the metal-host interaction. As we have previously shown,[42,43] the fluorescence displacement sensors function excellently in the presence of sodium-containing buffers such as PBS. However, mechanistic analysis of metal binding is simpler in the presence of a single metal, so Tris buffers were used here. The metal screen consisted of five general groups, as shown in Figure 2: alkaline earths (Ca^{2+}, Mg^{2+}), early transition metals (Mn^{2+} - Cu^{2+}), group IIB/IVA transition metals (Zn^{2+}, Cd^{2+}, Hg^{2+}, Pb^{2+}), rare earths (La^{3+}, Ce^{3+}, Er^{3+}) and actinides (Th^{4+}, UO_2^{2+}). Our preliminary test included 7 sensor elements: cavitands **1**-**3** [3 μM] with guest **4** [4 μM] at pH 5.0 and 7.4, and **5**•**1** at pH 7.4 ([**1**] = 20 μM, [**5**] = 1.5 μM). The relevant metal chloride salt at 50 μM (except for Th^{4+} and UO_2^{2+}, where the acetate was used) was added to each element, followed by monitoring the fluorescence changes. It was observed that three host:fluorophore combinations, **4**•**1** at both pH 5.5 and 7.4, and **5**•**1** at pH 7.4 gave the greatest signal changes. Fluorescence displacement/enhancement effects were observed with the cavitand **2**/**3**•guest **4** pairing, but the effects were more subtle (see Figure S-7 for the full screening data). As a result, we simplified the array design, employing only tetracarboxylate cavitand **1**. The results are shown in Figure 2, with the metals arranged from left to right in the order of increasing atomic number in each plot.

The largest fluorescence recovery (≥ 4-fold) was seen with guest **4** at pH 5.5 (Figure 2a) when the sensor was mixed with the lanthanides and actinides, La^{3+}, Ce^{3+}, Er^{3+}, and Th^{4+}. However, this sensor did not respond to the transition and main group metals, exhibiting little change in fluorescence. The same quenching effect by UO_2^{2+} was also observed at pH 7.4. Interestingly, the same sensor (3 μM **1**, 4 μM **4**, 20 mM Tris, Figure 2b) at the more basic pH of 7.4 displayed a very different response profile with greater variation in signal, with ~60% loss of fluorescence for early TMs, Cd^{2+}, Pb^{2+} and actinides, but minimal change for alkaline earths and Hg^{2+}, plus fluorescence *recovery* for the lanthanides. UO_2^{2+} was the only species that reduced the sensor fluorescence by 40~50% at both pH 5.5 and pH 7.4. The emission intensity of the DSMI: host complex **5**•**1** (20 μM **1**, 1.5 μM **5**, pH 7.4, 20 mM Tris) was decreased by the addition of metals (Figure 2c). Strong (almost 100%) loss of DSMI fluorescence enhancement was observed with Fe^{2+}, Co^{2+}, Ni^{2+}, Cu^{2+}, as well

as UO_2^{2+}, while the lanthanides and actinides induced loss in fluorescence varying from 30% (La^{3+}, Er^{3+}, Th^{4+}) to 70% (Ce^{3+}). Minimal change occurred to the sensor's fluorescence for alkaline earths, Mn^{2+} and the group IIB transition metals.

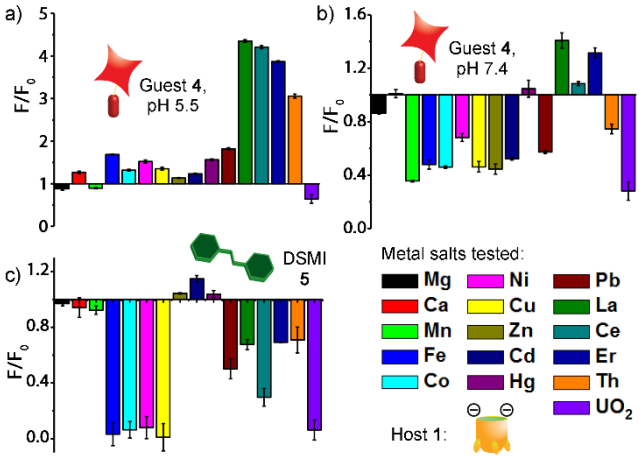

Figure 2. Fluorescence response change on metal addition to host:fluorophore complexes. [metal] = 50 μM; sensor **4•1**: [**1**] = 4 μM, [**4**] = 3 μM, in a) 20 mM Tris (pH 7.4) or b) Bis-Tris (pH 5.5) titrated to the corresponding pH with nitric acid; c) sensor **5•1**: [**1**] = 20 μM, [**5**] = 1.5 μM, in 20 mM Tris (pH 7.4).

The widely varying effects of addition of only micromolar amounts of metal ions on the fluorescence profile of the host:guest complexes are unusual and interesting. Importantly, the variation in sensor fluorescence is a *host*-mediated process: the fluorescence of guests **4** and **5** was not changed significantly upon addition of 50 μM metal in the absence of cavitand **1** (see Figure S-8). This makes sense: both guests **4** and **5** are cationic, and will have minimal contact with metal ions in aqueous solution at the low concentrations used. There was one exception, however: UO_2^{2+} showed strong native quenching of both **4** and **5** at pH 5.0 and 7.4, with ~ 20% and ~50% loss of fluorescence respectively.

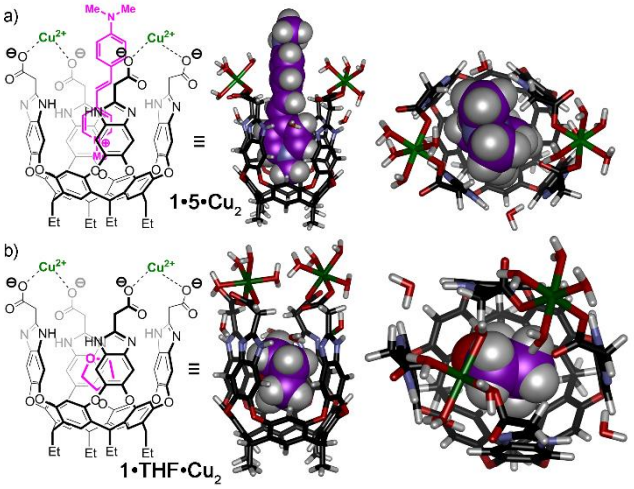

Figure 3. Minimized structures of a) **1•5•Cu**$_2$ and b) **1•THF•Cu**$_2$, indicating the effect on metal orientation in the presence of large and small guests (SPARTAN, AM1 forcefield).

The large signal change to the cavitand-guest system induced by the metals was unexpected, especially at micromolar concentrations in buffered water: host **1** only contains weakly coordinating carboxylate groups at the upper rim for metal complexation. Upon closer inspection of the structure (Figure 3), it becomes obvious that the carboxylate groups are in suitable proximity to each other to allow chelating interactions with large metal ions, increasing the target affinity.[56] Figure 3 shows minimized structures of complexes between host **1** and Cu^{2+} in the presence and absence of guests **4** and **5** (see Figure S-18 for the **1•4•Cu**$_2$ model). The freely rotating carboxylates allow bidentate metal binding in multiple orientations. In the presence of guest, the metals can be positioned away from the cavity. However, in the absence of the large fluorophore (Figure 3b), the metals reside above the cavity: metal complexation is possible in the presence of fluorophore, but lowers the fluorophore affinity due to steric interactions between the metal and the protruding guest. While these models are certainly not the only coordination modes possible (such as a 1:1 metal•cavitand complex, for example), they illustrate that metal coordination is tolerated by the **1•4** and **1•5** complexes and that the fluorophore affinity for **1** will be altered by metal binding. This also explains the minimal effect shown by small alkali and alkaline earth metals such as Mg^{2+} and Na^+: the small metals are less favorably chelated, and do not act as interferents.

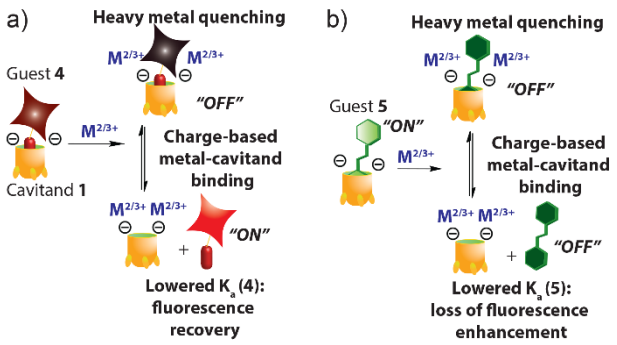

Figure 4. Illustration of the various sensing mechanisms involved in the recognition processes with the a) **1•4** and b) **1•5** complexes.

This modeling allows some conclusions to be drawn that explain the variable changes in response upon metal binding. The changes are subtle in some cases, and exact mechanistic analysis of each interaction is impractical, but some possibilities are illustrated in Figure 4. The analysis can be split into three separate cases - **1•4** at either pH 5.5 or pH 7.4, and **5•1**. The sensing of the metal in each case is mediated by the interaction of the newly added metal with the upper rim of the cavitand, and this effect is greatest for anionic **1** at pH 7.4. Guest **4** is strongly quenched by **1**, and its affinity is strongly pH-dependent.[43] Two competing factors are at play in the **4•1** system, which give competing responses (Figure 4a). The interaction of the added metal salt with the cavitand can bring this metal species into close proximity with bound **4**, causing additional quenching (and *lowered* fluorescence) via the heavy atom effect.[57] Alternatively, the metal interaction with **1** can interfere with the host:guest event, lessening the affinity of **4** for host **1**, releasing the guest into free solution and causing an *increase* in fluorescence. These two effects are both participating at pH 5.5 and 7.4, but the proportion of each effect varies. The fluorescence changes with the DSMI **5•1** sensor are different: in the majority of cases, a strong loss of fluorescence is observed upon addition of metal. The interactions of metal ions with host **1** are similar to those described as above, and the two competing mechanisms are still occurring. However, as DSMI shows enhanced fluorescence upon binding in **1**, both heavy metal-based quenching

of the **5•1** complex and expulsion of **5** from the cavitand upon host:metal interaction cause a loss of fluorescence enhancement in **5** (Figure 4b).

To corroborate these theories, calibration curves of fluorescence response vs. metal concentration were constructed for the metals that caused the most significant response ($F/F_{max} \geq 2$ or ≤ 0.5) in the three sensors: **1•4** at pH 5.5 or 7.4, and **1•5** at pH 7.4 (Figure S-9). Based on the potential interaction models proposed in Figure 4, we attempted to fit the curves with two simple binding models (see Experimental Section). The first model is the metal-cavitand-guest complex formation model, in which the titration curves of these metals were fitted with the Hill equation[52] by viewing the **1•4** complex as a single "macromolecule". The resultant macroscopic dissociation constant, labeled as "K_d^{MC}", serves as an index to compare the relative binding affinity of the metals to the **1•4** complex, as has been used for analysis of other host:guest indicator displacement systems.[20] The second model is the displacement model used for determination of inhibitor affinity to proteins.[58,59] This assay allows monitoring of ligand displacement from the protein-ligand complex by small molecule inhibitors, and this fitting gives the dissociation constant of the metal-cavitand complex, marked as K_d^D. These simple models may not reflect the complete binding situation, because the final fluorescence changes depend on multiple binding events, including the strength of the **1**•M^{2-4+} interaction and the efficiency of the guest quenching by the metal. However, the responses for certain metals are dominated by a single interaction type, and are amenable to fitting by one of the simple models.

Table 1: Metal Affinity Constants for the **4•1** Complex Sensor.[a]

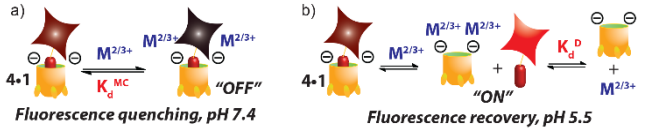

Metal	K_d^{MC}, μM	n
Fe^{2+}	3.8±1.4	2.1
Co^{2+}	2.0±0.4	2.7
Zn^{2+}	2.7±0.8	2.0
Cu^{2+}	0.7±0.1	1.4
Cd^{2+}	2.5±0.3	2.3
Pb^{2+}	1.3±0.3	2.0
UO_2^{2+}	1.4±0.2	1.1

Metal	K_d^D, μM
La^{3+}	1.0±0.1
Ce^{3+}	1.1±0.1
Er^{3+}	0.9±0.1
Th^{4+}	1.1±0.1

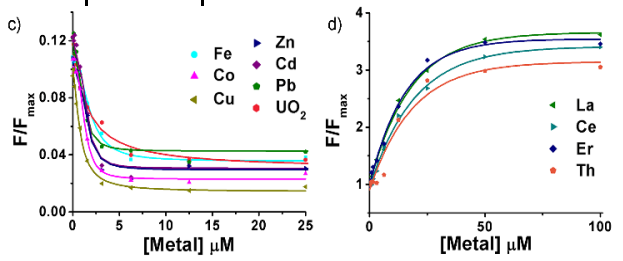

[a][**1**] = 3 μM, [**4**] = 4 μM, pH 7.4, 20 mM Tris. K_d^{MC} determined via Hill equation,[52] K_d^D determined *via* enzyme inhibitor model.[58] c) calibration curves for Hill analysis; d) calibration curves for inhibitor analysis.

At pH 7.4, the early transition metals (Mn^{2+} - Zn^{2+}), the heavy metals (Pb^{2+} and Cd^{2+}), as well as UO_2^{2+}, reduced the **1•4** sensor fluorescence by more than 50%, indicating that formation of the stable **M^{2+}•1•4** complex could be the dominant effect. Indeed, fitting the binding curves to the Hill equation was successful with $R^2 = 0.99$ (Table 1a,c; Figure S-10), while the no fit was seen with the displacement model. The tested metals all showed a positive cooperativity "n" between 1 and 2, indicating that binding of the first metal cation could facilitate the binding of the subsequent ions. The K_d^{MC} values were relatively consistent, ranging from 0.7±0.1 μM (Cu^{2+}) to 3.8±1.4 μM (Fe^{2+}). The strong affinity of these metals to the **1•4** complex is expected, as host **1** will display (on average) a bis-anionic charge under these conditions, allowing strong charge matching with the metal cations. This strong binding was also persistent and observable in mass spectrometry: both Cu^{2+} and UO_2^{2+} formed stable complexes with cavitand **1**, detectible by surface-enhanced laser desorption/ionization (SELDI) assisted with graphene oxide (see Figure S-14). The MS data clearly showed that these two cations could coordinate with cavitand **1** at 1:1, 2:1, and 3:1 stoichiometries, when mixing 10 μM of cavitand **1** and 100 μM of the metal cation. At pH 5.5, only the lanthanides induced sufficiently large fluorescence enhancement of the **1•4** sensor to allow fitting (Table 1b,d, Figure S-11). These binding curves fit well with the displacement model, resulting in K_d^D values around 1 μM, consistent with the theory that fluorescence enhancement occurs via displacement of **4** and concomitant loss of quenching. The K_d^D values may not represent the true dissociation constant between metal and cavitand, because of the overly simplified assumption of a 1:1 binding stoichiometry, but this analysis corroborates the fluorophore displacement concept. The oxophilic Ln^{3+} ions are the only ions capable of strong affinity for **1** in its partially protonated state.

Table 2: Metal Affinity Constants for the **5•1** Complex Sensor.[a]

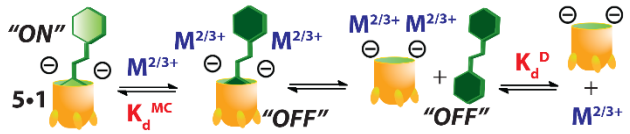

Metal	K_d^{MC}, μM	n	K_d^D, μM
Fe^{2+}	58 ± 14	2	N/A
Co^{2+}	200 ± 40	2.7	N/A
Ni^{2+}	73 ± 14	2.5	N/A
Cu^{2+}	8.7 ± 1.7	1.6	N/A
Pb^{2+}	$(1.3\pm0.3)\times10^3$	1.5	12.2±1.7
Ce^{3+}	$(1.9\pm0.6)\times10^3$	2.3	2.7±0.1
UO_2^{2+}	4.9 ± 0.5	1.1	N/A

[a][**1**] = 20 μM, [**5**] = 1.5 μM, pH 7.4, 20 mM Tris. K_d^{MC} determined via Hill equation,[52] K_d^D determined *via* enzyme inhibitor model.[58] Red = best fit with the inhibitor model.

The analysis of the DSMI **5•1** sensor was more complex. Since we could not determine whether complex formation or displacement were the contributing factors (as both mechanisms cause guest **5** quenching), we fitted the binding curves of the ions that induce > 50% fluorescence reduction (the early transition metals (Fe^{2+}-Cu^{2+}), Pb^{2+}, Ce^{3+}, and UO_2^{2+}) with both models. Interestingly, fitting to the

Hill equation was more successful than the displacement model (Table 2; Figure S-12). The K_d^{MC} values ranged from ranging from 8.7±1.7 μM (Cu^{2+}) to 1.9±0.6 mM (Ce^{3+}), indicating much greater variance in binding affinity for the **5•1** sensor than with the **4•1** sensor. Only Pb^{2+} and Ce^{3+} showed good fitting with the displacement model. The large K_d^{MC} values found for these two cations using the complex formation model indicated the relatively low stability of the $\mathbf{M^{2+}•1•5}$ complex, displacing guest **5** due to the high affinity of the metal for the host.

The calibration curves typically exhibit linear response ranges between 0-10 or 0-20 μM, before reaching plateau at higher metal concentration. Using the linear regression equation and the 3σ method, the limits of detection (LOD) of each sensor for individual metals were found to be between 1.2-0.07 μM, with a linear range (see Figure S-13). The lowest LOD of 0.07 μM is observed for Cu^{2+} with the **4•1** sensor at pH 7.4. The LOD of heavy metals ranges from 1.3 (Th^{4+}) to 0.31 μM (Er^{3+}) with the **1•4** sensor at pH 5.5. The limit of quantitation (LOQ, calculated using the 10σ method, see Figure S-16) for either the cation (Ce^{3+} or Th^{4+}) alone, or the mixture of $La^{3+}/Er^{3+}/Ce^{3+}/Th^{4+}$ at equal molarity were quite similar, around 1-2 μM, even when spiked in the environmental water sample collected from Lake Evans, Riverside, CA.

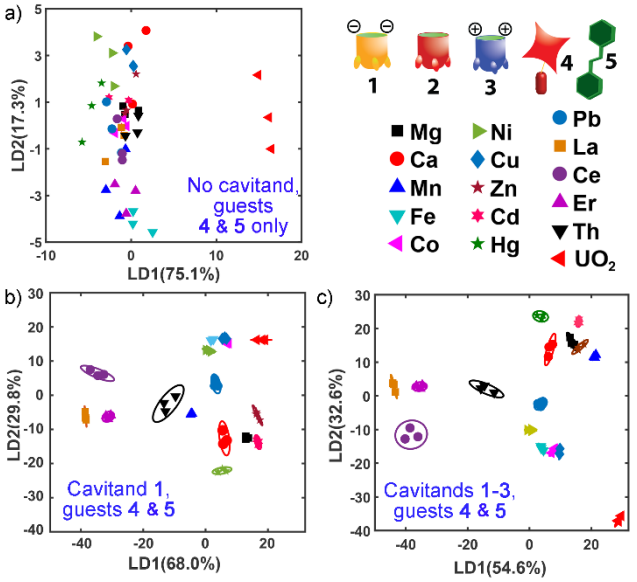

Figure 5. Metal salt identification *via* Linear Discriminant Analysis. a) Scores plot of the metal screen with a cavitand-free screen, [**4**] = 3 μM, [**5**] = 1.5 μM; b) Scores plot of the metal screen with the 3 factor sensor array containing **4•1** ([**1**] = 4 μM, [**4**] = 3 μM) in pH 7.4 or pH 5.5 buffer, and sensor **5•1** ([**1**] = 20 μM, [**5**] = 1.5 μM, pH 7.4); c) Scores plot of the metal screen with the 7 factor sensor array containing **4•1/4•2/4•3** ([**1**] = 4 μM, [**2**] = 3 μM, [**3**] = 3 μM, [**4**] = 3 μM) in pH 7.4 or pH 5.5 buffer, and sensor **5•1** ([**1**] = 20 μM, [**5**] = 1.5 μM, pH 7.4). pH 7.4 = 20 mM Tris, pH 5.5 = 20 mM Bis-Tris.

The multiple different interactions and quenching mechanisms between the various metals and sensor components are ideal for analysis by discriminant methods. Each sensor responds to multiple metals, which induces subtle fluorescence changes sensitive to the type and concentration of the metals. Linear discriminant analysis (LDA)[10] was chosen as the discriminant technique here, as it can yield dimensional components optimized to maximize the differentiation among sample classes, as opposed to unsupervised pattern recognition tools like principal component analysis (PCA).[10] As a baseline control, the fluorescence profiles obtained by incubating the metal salts on free, uncomplexed guests **4** and **5** were subjected to LDA (Figure 5a). As expected, the fluorophores are incapable of effectively discriminating the metal salts in the absence of cavitand. The only outlier is UO_2^{2+}, which can be easily identified in the scores plot, due to its strong native quenching ability. All other metals, including light and heavy metals are unclustered and indistinguishable.

In contrast, when only a 3-component cavitand:fluorophore sensor array was used, excellent discrimination of almost all the metal ions can be achieved. When LDA was applied to the data set from Figure 2 (with **4•1** at pH 5.5/7.4, and **5•1**), the scores plot shown in Figure 5b is obtained. In each case, three repeats were taken for each sample, and these three repeated measurements of the same metal were included well within the 95% confidence ellipses, showing good reproducibility of our measurement. The not-overlapping ellipses reveal good separation of different metals by our sensor array. Most importantly, the metals with the highest structural similarity, i.e. La^{3+}, Ce^{3+}, Er^{3+}, and Th^{4+}, are extremely well-separated from each other. In addition, the scores plot shows three main clusters of metals. All the lanthanides are located in the left panel on the scores plot (LD1 < 0), away from the other metals which displayed LD1 > 0. The upper right panel (LD2 >0) was occupied by the early transition metals metals $Fe^{2+}/Co^{2+}/Ni^{2+}/Cu^{2+}$ and the outlier UO_2^{2+}, while the lower right panel (LD2 < 0) contained mainly the IIA/ IIB metals ($Mg^{2+}/Ca^{2+}/Zn^{2+}/Cd^{2+}/Hg^{2+}$).

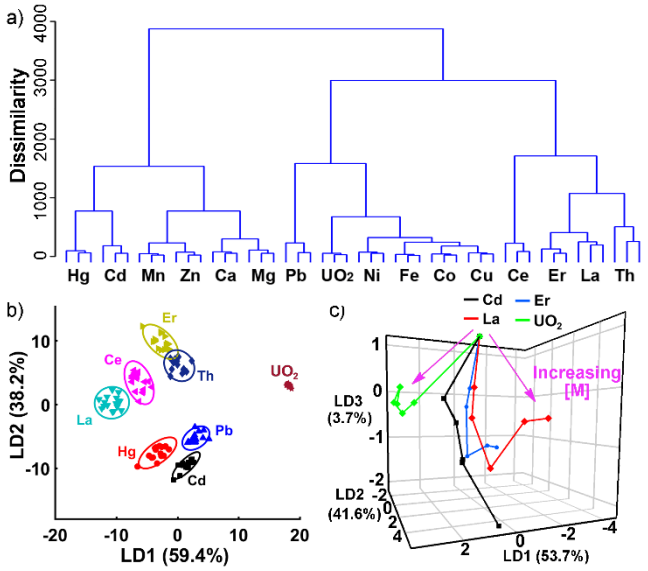

Figure 6. a) Hierarchical cluster analysis; b) metal identification and c) quantification by the 3 factor sensor array containing **4•1** ([**1**] = 4 μM, [**4**] = 3 μM) in 20 mM Tris (pH 7.4) or Bis-Tris (pH 5.5) buffer, and sensor **5•1** ([**1**] = 20 μM, [**5**] = 1.5 μM, in 20 mM Tris, pH 7.4). [Metal] in (c) = 0, 0.8, 1.6, 3.1, 6.3, 12.5, 25.0, 50.0, 100.0 μM.

The full 7-factor sensor array was also applied to the metal screen, and the LDA scores plot is shown in Figure 5c. This array included four more variables, the sensors formed by the neutral and cationic cavitands **2** and **3** with the rhodamine guest **4** at two pHs. While the individual effects of these hosts were much more subtle, the array with more variables was more tolerant to random signal variation, and thus the 95% ellipses enclosing the three repeats of each metal were much narrower. The extended array still gave out excellent sep-

aration among the trivalent inner transition metals, with some improvement in the discrimination of the VIIIB/IB metals. However, Pb^{2+} and Mn^{2+} were much closer to the IIA/IIB cluster and the separation among the metals within this cluster were poorer.

The metal discrimination was also tested with Hierarchical Cluster Analysis (HCA) on the simple 3-factor sensor. On the resultant dendrogram (see Figure 6a), all three repeats for the same metal were clustered well with very small dissimilarity (< 100), and three main clusters with dissimilarity close to 2,000 were found: the VIIIB/IB metals (Fe^{2+}/Ni^{2+}/Co^{2+}/Cu^{2+}), the IIA/IIB groups (Ca^{2+}/Mg^{2+} /Zn^{2+}/Hg^{2+}/Cd^{2+}), and the inner transition metals (La^{3+}/Ce^{3+}/Er^{3+}/Th^{4+}). Pb^{2+} and UO_2^{2+} were clustered with the VIIIB/IB metals, and Mn^{2+} was included in the IIA/IIB group, agreeing with their relative locations on the LDA score plot. Both the LDA and HCA results support that the observed fluorescence profiles are closely related to metal properties. Even with just three array variables, the simple sensor system can not only discriminate between metals with different coordination behavior, but can also discriminate between highly similar metals while allowing their grouping and analysis. To further evaluate the simple 3-component sensor capabilities for the discrimination of environmentally relevant heavy metals (Hg^{2+}, Cd^{2+}, Pb^{2+}) and the lanthanides/actinides (UO_2^{2+}, La^{3+}, Er^{3+}, Ce^{3+}, Th^{4+}), we performed a more detailed analysis of these species. Figure 6b shows the score plot from LDA of these 8 metals, with significantly more repeats (n = 16). Despite the extensive number of repeats used, the 95% ellipses showed either zero or minimal (Er^{3+}/Th^{4+}) overlap on the score plot, meaning that these metals can be differentiated with 95% confidence using our sensor array coupled with LDA. In addition, Jackknife analysis showed that each metal can be assigned to the correct group with 100% accuracy (see Table S-1).

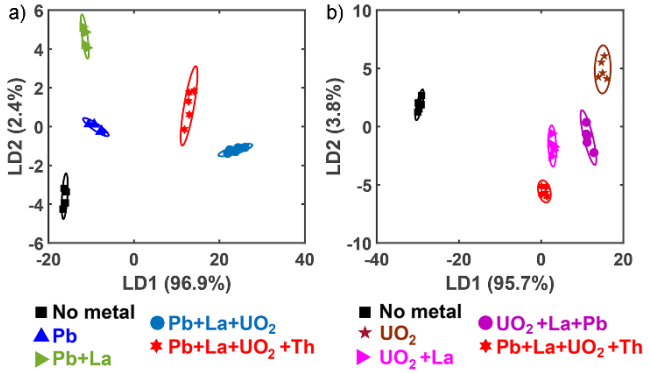

Figure 7. Metal salt identification in Mixtures. LDA Scores plots identifying a) Pb^{2+}; b) UO_2^{2+} in the presence of other salts in commercial tap water with the three factor sensor array containing **4•1** ([**1**] = 4 μM, [**4**] = 3 μM) in pH 7.4 or pH 5.5 buffer, and sensor **5•1** ([**1**] = 20 μM, [**5**] = 1.5 μM, pH 7.4). [Metal] = 20 μM, pH 7.4 = 20 mM Tris, pH 5.5 = 20 mM Bis-Tris.

Of course, the most important and challenging task is to detect these metals in a complex mixture of ions, as would be observed in an environmental sample. Quantifying one metal ion in the presence of other metal ions is challenging without pre-treatment and sophisticated instruments like ICP-AES or ICP-MS, due to the cross-reactivity between the recognition probes. Metal quantitation using our array was tested by measuring the fluorescence responses with increasing concentrations of each metal when mixed with the sensors. Indeed, when the metal concentration increased from 0 to 100 μM in tap water, the position of the sample on the 3D-score plot resulted from LDA of the fluorescence profiles would move towards different directions depending on the identity of the metal (Figure 6c). Increasing metal concentrations moved all samples downward in the LD3 direction, but different metals projected toward different direction on the LD1-LD2 plane. For instance, increasing [Cd^{2+}] moved the location of the metal sample to a more positive LD2 location with little change in LD1, while higher [UO_2^{2+}] moved it towards more positive LD1 and more negative LD2 with small change in LD3 direction. No overlap was observed between the trajectories of individual metals, indicating good capability of sensor in recognizing the elevated concentration of one metal in tap water. This confirms that the array is capable of quantitating the heavy and inner transition metals in aqueous solutions.

Table 3: Metal Mixture Analysis in Environmental Sample[a]

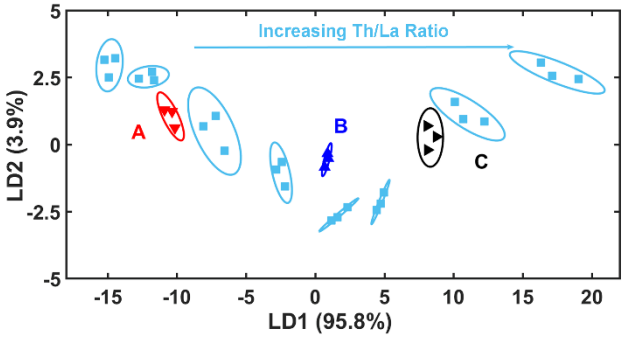

Entry	[Th^{4+}], μM			[La^{3+}], μM		
	Actual	ICP-AES	Array	Actual	ICP-AES	Array
A	4.5	4.3	3-6	16.5	16.6	15-18
B	10.2	10.3	9-12	10.8	11.1	9-12
C	16.3	16.3	15-18	4.7	4.7	3-6

[a] Quantifying the binary mixture of La^{3+}/Th^{4+} with the ratio of these two ions changing from 0:21 to 21:0 in 3 μM increments, with the three factor sensor array in natural lake water, containing **4•1** ([**1**] = 4 μM, [**4**] = 3 μM) in pH 7.4 or pH 5.5 buffer, and sensor **5•1** ([**1**] = 20 μM, [**5**] = 1.5 μM, pH 7.4). pH 7.4 = 20 mM Tris, pH 5.5 = 20 mM Bis-Tris. A, B, and C are the test samples. Performance of quantification compared with ICP-AES.

To illustrate the efficacy of the sensor towards environmentally relevant mixtures, we prepared a series of samples with increasing complexity. The first set of samples was created by spiking several metals, each with a final concentration of 2 μM, to unpurified tap water and testing the samples with our 3-factor sensor array, with a focus on detecting the environmentally important ions Pb^{2+} and UO_2^{2+} in mixtures containing the similarly sized metals at comparable molarity. As tap water contains small amounts of the small metals (Mg^{2+}, Ca^{2+}, Fe^{2+}) already, we focused on the detection of heavy metals and the challenging discrimination between heavy metals of similar sizes. The fluorescence patterns were subject to LDA and the resultant score plots were shown in Figure 7 (the score plot with 11 mixtures displayed in Figure S-15; raw fluorescence data in Figure S-17). We can see from Figure 7a that the co-presence of the inner transition metals like La^{3+}, Th^{4+}, and UO_2^{2+}, with Pb^{2+} were well differentiated

from each other. Similarly, if the tap water contained higher contents of inner transition metals, the simple array can recognize the different combinations of La^{3+}, Th^{4+}, and UO_2^{2+} in the water samples. Jackknife analysis also showed that various mixtures can be assigned to the correct group with 100% accuracy (see Table S-2).

The second set of samples was created by spiking La^{3+} and Th^{4+} at various molar ratios (La^{3+}:Th^{4+} = 0:21, 3:18, 6:15, 9:12, 12:9, 15:6, 18:3, 21:0, all in μM), to lake water obtained from Lake Evans, Riverside, CA. Three analytic samples were prepared for comparison: **A** – (16.5 μM La^{3+} + 4.5 μM Th^{4+}); **B** (10.8 μM La^{3+} + 10.2 μM Th^{4+}) and **C** (4.7 μM La^{3+} + 16.3 μM Th^{4+}). LDA was applied to the data collected from the test samples and the standard mixtures. We can see on the resultant scores plot that the test samples locate in the correct location, corresponding to their metal ratios. For example, sample A located in between the two standards with La^{3+}:Th^{4+} molar ratios at 15:6 and 18:3 respectively. This location indicates that it contains 15-18 μM La^{3+} and 3-6 μM Th^{3+}. This range agrees with what was detected by ICP-AES. Table 3 shows the full detection data, and illustrates the ability of the array to semi-quantitatively detect the presence of heavy metals in complex environmental samples. The simple optical array is an effective, quick survey method comparable to ICP-AES analysis without the expense.

Conclusions

Here, we have shown that a simple three component host:fluorophore sensor array is capable of sensing and discriminating aqueous solutions of metal salts. Excellent sensitivity is possible, and highly similar metals such as lanthanides and actinides can be easily distinguished at low micromolar concentrations in complex salt mixtures. The statistical analysis is robust and simply performed using common computational software, and allows highly sensitive discrimination of similar heavy metals, such as the rare earth metals that display almost identical charges and coordination spheres. Multiple coordination and fluorescence quenching/enhancement mechanisms occur in the system, which contributes to the sensitivity of the discrimination. This flexible, yet simple sensor array represents a powerful tool for monitoring heavy or RE metal pollution in the environment in a quick, low-cost, and high-throughput manner, which is essential for prompt pollution control and treatment implementation

ASSOCIATED CONTENT

Supporting Information

Additional fluorescence and absorbance data, full LDA plots and statististical analysis, calibration curves and MS analysis data. This material is available free of charge via the Internet at http://pubs.acs.org.

AUTHOR INFORMATION

Corresponding Authors

* Phone: +1 951 827 4924. Fax: +1 951 827 4713.
E-mail: richard.hooley@ucr.edu; wenwan.zhong@ucr.edu

ACKNOWLEDGMENTS

The authors would like to thank the National Science Foundation (CHE-1748063 to W.Z. and R.J.H.), and the UC Riverside Office of Research and Development (Collaborative Seed Grant to W.Z.) for the support.

REFERENCES

(1) Weiss, D. J.; Rehkaemper, M.; Schoenberg, R.; McLaughlin, M.; Kirby, J.; Campbell, P. G. C.; Arnold, T.; Chapman, J.; Peel, K.; Gioia, S. *Environ. Sci. Technol.* **2008**, *42*, 655-663.
(2) Traudt, E. M.; Ranville, J. F.; Meyer, J. S., *Environ. Sci. Technol.* **2017**, *51*, 4471-4481.
(3) Nys, C.; Versieren, L.; Cordery, K. I.; Blust, R.; Smolders, E.; De Schamphelaere, K. A. C. *Environ. Sci. Technol.* **2017**, *51*, 4615-4623.
(4) Donohue, D. L. *Anal. Chem.* **2002**, *74*, 28A-35A.
(5) Steinhauser, G. *Environ. Sci. Technol.* **2014**, *48*, 4649-4663.
(6) Shen, Y.; Fang, Q.; Chen, B. *Environ. Sci. Technol.* **2015**, *49*, 67-84.
(7) Zhang, P.; Chen, Y.-P.; Wang, W.; Shen, Y.; Guo, J.-S. *Trends Anal. Chem.; TrAC* **2016**, *85*, 153-165.
(8) Zhou, W.; Saran, R.; Liu, J. *Chem. Rev.* **2017**, *117*, 8272-8325.
(9) Yuen, L. H.; Franzini, R. M.; Tan, S. S.; Kool, E. T. *J. Am. Chem. Soc.* **2014**, *136*, 14576-14582.
(10) Tan, S. S.; Kim, S. J.; Kool, E. T. *J. Am. Chem. Soc.* **2011**, *133*, 2664-2671.
(11) Yuen, L. H.; Franzini, R. M.; Wang, S.; Crisalli, P.; Singh, V.; Jiang, W.; Kool, E. T., *Angew. Chem. Int. Ed.* **2014**, *53*, 5361-5365.
(12) Huang, P.-J. J.; Vazin, M.; Lin, J. J.; Pautler, R.; Liu, J. *ACS Sensors* **2016**, *1*, 732-738.
(13) Gao, L.; Li, L.-L.; Wang, X.; Wu, P.; Cao, Y.; Liang, B.; Li, X.; Lin, Y.; Lu, Y.; Guo, X., *Chem. Sci.* **2015**, *6*, 2469-2473.
(14) Zhan, S.; Wu, Y.; Wang, L.; Zhan, X.; Zhou, P., *Biosens. Bioelectron.* **2016**, *86*, 353-368.
(15) Huang, P.-J. J.; Lin, J.; Cao, J.; Vazin, M.; Liu, J. *Anal. Chem.* **2014**, *86*, 1816-1821.
(16) Huang, P.-J. J.; Vazin, M.; Liu, J. *Anal. Chem.* **2014**, *86*, 9993–9999.
(17) Wu, C.-S.; Oo, M. K. K.; Fan, X. *ACS Nano* **2010**, *4*, 5897-5904.
(18) Cui, L.; Wu, J.; Ju, H., *Biosens. Bioelectron.* **2015**, *63*, 276-286.
(19) Saidur, M. R.; Aziz, A. R. A.; Basirun, W. J., *Biosens. Bioelectron.* **2017**, *90*, 125-139.
(20) Bakirci, H.; Koner, A. L.; Nau, W. M. *Chem. Commun.* **2005**, 43, 5411-5413.
(21) Aoki, S.; Kagata, D.; Shiro, M.; Takeda, K.; Kimura, E. *J. Am. Chem. Soc.* **2004**, *126*, 13377-13390.
(22) Gorden, A. E. V.; DeVore, II, M. A.; Maynard, B. A. *Inorg. Chem.* **2013**, *52*, 3445-3458.
(23) Panak, P. J.; Geist, A. *Chem. Rev.* **2013**, *113*, 1199-1236.
(24) Schwochau, K. *Top. Curr. Chem.* **1984**, *124*, 91-133.
(25) Balonov, M.; et al. *Radiological Conditions in the Dnieper River Basin*; Radiological Assessment Reports Series; International Atomic Energy Agency: Vienna, 2006.
(26) Sather, A.C.; Berryman, O. B.; Rebek, J., Jr. *J. Am. Chem. Soc.* **2010**, *132*, 13572–13574.
(27) Palacios, M. A.; Wang, Z.; Montes, V. A.; Zyryanov, G. V.; Anzenbacher, P. *J. Am. Chem. Soc.* **2008**, *130*, 10307-10314.
(28) Hewage, H. S.; Anslyn, E. V. *J. Am. Chem. Soc.* **2009**, *131*, 13099-13106.
(29) Kitamura, M.; Shabbir, S. H.; Anslyn, E. V. *J. Org. Chem.* **2009**, *74*, 4479-4489.
(30) Lee, J. W.; Lee, J.-S.; Kang, M.; Su, A. I.; Chang, Y.-T., *Chem. Eur. J.* **2006**, *12*, 5691-5696.
(31) Xu, W.; Ren, C.; Teoh, C. L.; Peng, J.; Gadre, S. H.; Rhee, H.-W.; Lee, C.-L. K.; Chang, Y.-T. *Anal. Chem.* **2014**, *86*, 8763-8769.
(32) Wang, Z.; Palacios, M. A.; Anzenbacher, P. *Anal. Chem.* **2008**, *80*, 7451-7459.
(33) Mayr, T.; Igel, C.; Liebsch, G.; Klimant, I.; Wolfbeis, O. S. *Anal. Chem.* **2003**, *75*, 4389-4396.
(34) Jurs, P.C.; Bakken, G.A.; McClelland, H.E. *Chem. Rev.* **2000**, *100*, 2649–2678.
(35) Stewart, S.; Ivy, M. A.; Anslyn, E. V. *Chem. Soc. Rev.* **2014**, *43*, 70-84.

(36) Biros, S. M.; Ullrich, E. C.; Hof, F.; Trembleau, L.; Rebek, J. *J. Am. Chem. Soc.* **2004**, *126*, 2870-2876.
(37) Liu, Y.; Liao, P.; Cheng, Q.; Hooley, R.J. *J. Am. Chem. Soc.* **2010**, *132*, 10383-10390.
(38) Liu, Y.; Young, M.C.; Moshe, O.; Cheng, Q.; Hooley, R.J. *Angew. Chem. Int. Ed.* **2012**, *51*, 7748-7751.
(39) Ghang, Y.-J.; Schramm, M.P.; Zhang, F.; Acey, R.A.; David, C.N.; Wilson, E.H.; Wang, Y.; Cheng, Q.; Hooley, R.J. *J. Am. Chem. Soc.* **2013**, *135*, 7090-7093.
(40) Li, V.; Ghang, Y.-J.; Hooley, R.J.; Williams T.J. *Chem. Commun.* **2014**, *50*, 1375 - 1377.
(41) Perez, L.; Mettry, M.; Hinman, S.S.; Byers, S. R.; McKeating, K.S.; Caulkins, B.G.; Cheng, Q.; Hooley, R.J. *Soft Matter* **2017**, *13*, 3966 - 3974.
(42) Liu, Y.; Perez, L.; Mettry, M.; Easley, C. J.; Hooley, R. J.; Zhong, W. *J. Am. Chem. Soc.* **2016**, *138*, 10746-10749.
(43) Liu, Y.; Perez, L.; Mettry, M.; Gill, A. D.; Byers, S. R.; Easley, C. J.; Bardeen, C. J.; Zhong, W.; Hooley, R. J. *Chem. Sci.* **2017**, *8*, 3960- 3970.
(44) You, L.; Zha, D.; Anslyn, E.V. *Chem. Rev.* **2015**, *115*, 7840−7892.
(45) Ghale, G.; Nau, W.M. *Acc. Chem. Res.* **2014**, *47*, 2150−2159.
(46) Umali, A. P.; Anslyn, E.V. *Curr. Opin. Chem. Biol.* **2010**, *14*, 685–692.
(47) Wright, A.T.; Anslyn, E.V.; McDevitt, J.T. *J. Am. Chem. Soc.* **2005**, *127*, 17405-17411.
(48) Minaker, S.A.; Daze, K.D.; Ma, M.C.F.; Hof, F. *J. Am. Chem. Soc.* **2012**, *134*, 11674−11680.
(49) Peacor, B. C.; Ramsay, C. M.; Waters, M. L. *Chem. Sci.* **2017**, 8, 1422-1428.
(50) Rafai Far, A.; Shivanyuk, A.; Rebek, J., Jr. *J. Am. Chem. Soc.* **2002**, *124*, 2854-2855.
(51) Soberats, B.; Sanna, E.; Martorell, G.; Rotger, C.; Costa, A. *Org Lett.* **2014**,*16*, 2480-2483.
(52) de la Peña, A. M.; Salanas, F.; Gómez, M. J.; Acedo, M. I.; Peña, M. S. *J. Inclus. Phenom. Mol. Rec. Chem.* **1993**, *15*, 131-143.
(53) Korbakov, N.; Timmerman, P.; Lidich, N.;Urbach, B.; Sa'ar, A.; Yitzchaik, S. *Langmuir* **2008**, *24*, 2580-2587.
(54) Fernández-Abad, S.; Pessêgo, M.; Basílio, N.; García-Río, L. *Chem. Eur. J.* **2016**, *22*, 6466 – 6470.
(55) Sun, S.; Yuan, Y.; Li, Z.; Zhang, S.; Zhang, H.; Peng, X. *New J. Chem.* **2014**, *38*, 3600-3605.
(56) Mettry, M.; Moehlig, M.P.; Hooley, R.J. *Org. Lett.* **2015**, *17*, 1497-1500.
(57) Shimizu, Y.; Azumi, A. *J. Phys. Chem.*, **1982**, *86*, 22–26.
(58) Hulme, E.C.; Birdsall, N.J.M. Strategy and Tactics in Receptor-Binding Studies. In *Receptor–Ligand Interactions: A Practical Approach*, Hulme, E.C. ed., Oxford University Press, 1992, pp 63–176.
(59) Cer, R. Z.; Mudunuri, U.; Stephens, R.; Lebeda, F. J. *Nucleic Acids Res.* **2009**, W441–W445.

For TOC Only:

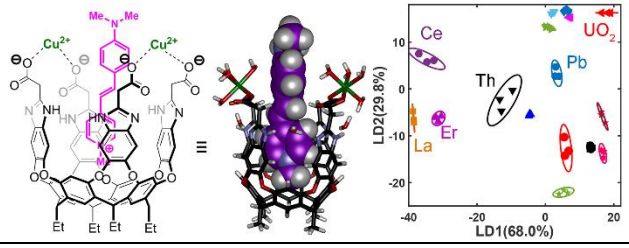
Me
N
Me
Cu2+
Cu2+
NH
HN
HN
N
HN
N
Et
Et
Et
Et
≡
Ce
UO2
Pb
Th
Er
La
LD2(29.8%)
LD1(68.0%)
10
0
-10
-20
-40
-20
0
20

Supporting Information

Selective Heavy Element Sensing with a Simple Host:Guest Fluorescent Array

Yang Liu,[2] Magi Mettry,[1] Adam D. Gill,[3] Lizeth Perez,[1] Wenwan Zhong[1,2] and Richard J. Hooley[1,3]**

[1]Department of Chemistry; [2]Environmental Toxicology Program; [3]Department of Biochemistry and Molecular Biology; University of California-Riverside, Riverside, CA 92521, U.S.A.

richard.hooley@ucr.edu; wenwan.zhong@ucr.edu

Table of Contents

Calculation of the fraction of the bound guest in each sensor

Using the K_d of guest (G)-cavitand (Cav), we can solve the binding equilibrium and calculate the fraction of the bound fluorescent guest in the solution prior to mixing with different metal ions:

$$K_d = \frac{[Cav]\times[G]}{[Cav\cdot G]} \qquad (1)$$

$$[Cav] = [Cav]_0 - [Cav \cdot G] \qquad (2)$$

$$[G] = [G]_0 - [Cav \cdot G] \qquad (3)$$

Then,

$$K_d = \frac{([Cav]_0-[Cav\cdot G])\times([G]_0-[Cav\cdot G])}{[Cav\cdot G]} \qquad (4)$$

Solve for $[Cav \cdot G]$, which is the roots of above quadratic equation.

We found the following ratios:

For DSMI, the ratio of [complex]/[Total DSMI] = 45.6%

For RhB 7.4, the ratio of [complex]/[Total RhB] = 59.5%

For RhB 5.5, the ratio of [complex]/[Total RhB] = 80.0%.

Supporting Figures

1. Guest 5 (DSMI) Optical Properties

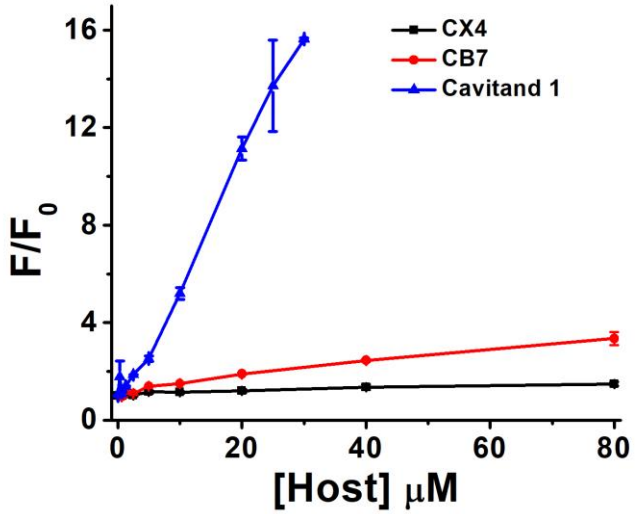

Figure S-1. Increase of DSMI **5** fluorescence upon binding to three synthetic hosts, **CX4** (tetrasulfonatocalix[4]arene), **CB7** (cucurbit[7]uril) and cavitand **1**. [DSMI **5**] = 1.5 μM in 20 mM Tris, pH =7.4.

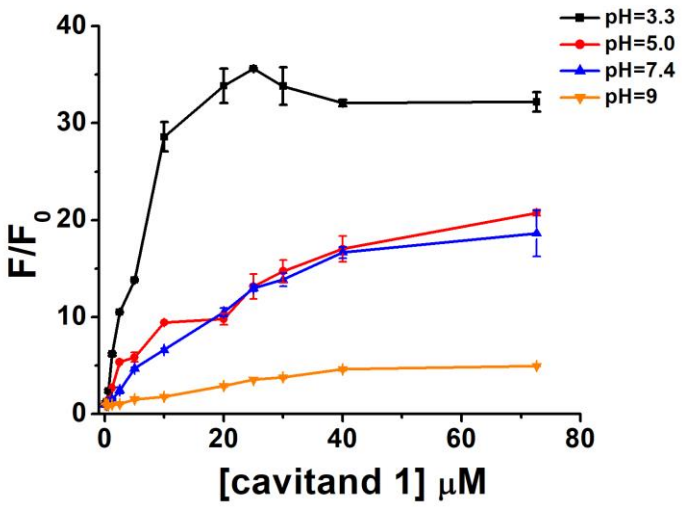

Figure S-2. Increase of DSMI **5** fluorescence upon binding to cavitand **1** under various pH values. [DSMI **5**] = 1.5 μM in 50 mM citrate (pH 3.3), phosphate (pH 5.0 and pH 7.4), or carbonate (pH 9.0) buffer.

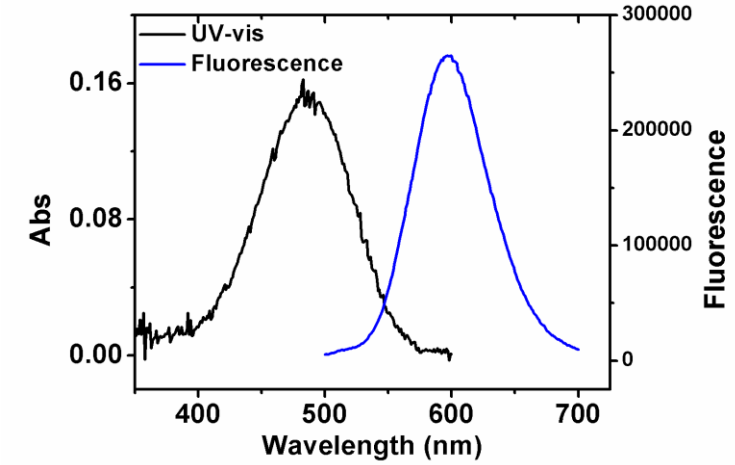

Figure S-3. UV-Vis absorption and fluorescence emission (with λ_{ex} = 485 nm) spectra of the complex formed between cavitand **1** (20 μM) and DSMI **5** (5 μM) in 50 mM Tris, pH 7.4. The maximum λ_{abs} was found to be 485 nm which was used to excite the fluorescence of DSMI in the following experiments, and fluorescence emission was collected at λ = 605 nm, judged by the emission spectrum presented here.

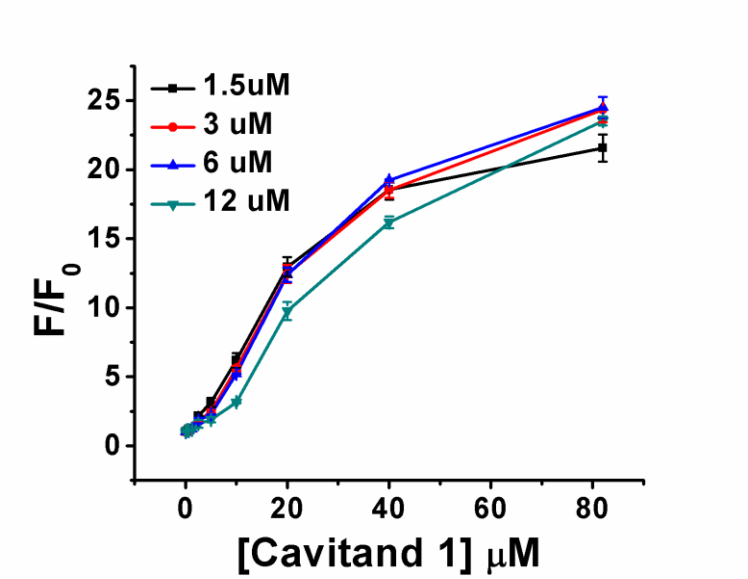

Figure S-4. Fluorescence change ratio when mixing 1.5, 3, 6, and 12 μM of DSMI **5** with increasing concentrations of cavitand **1**. The combination of 1.5 μM DSMI **5** and 20 μM cavitand **1** was chosen to compose the metal sensing array.

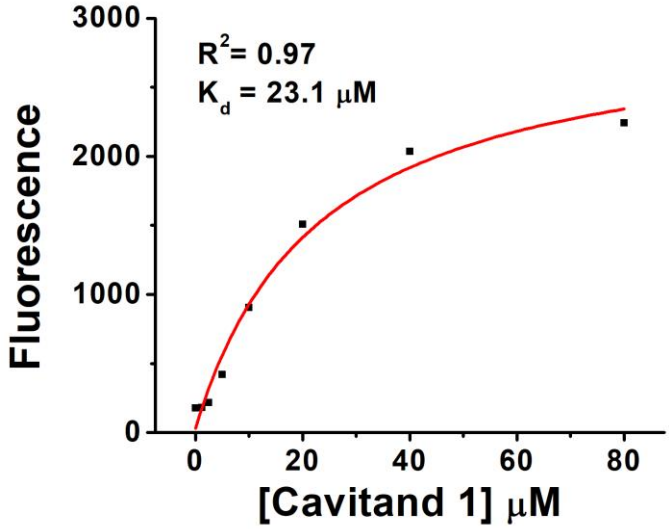

Figure S-5. The binding curve of **1•5** fitted with the following equation to obtain the dissociation constant of **1•5**:[1]

$$\frac{F}{F_0} = 1 + \left(\frac{F_{max}}{F_0} - 1\right) \frac{1/K_d\,[host]}{1+1/K_d[host]} \qquad (5)$$

where F = Fluorescence, F_0 = Fluorescence with cavitand, F_{max} = Fluorescence without cavitand, K_d = dissociation constant, [*host*] = cavitand concentration. [DSMI **5**] = 5 μM in 50 mM Tris at pH =7.4.

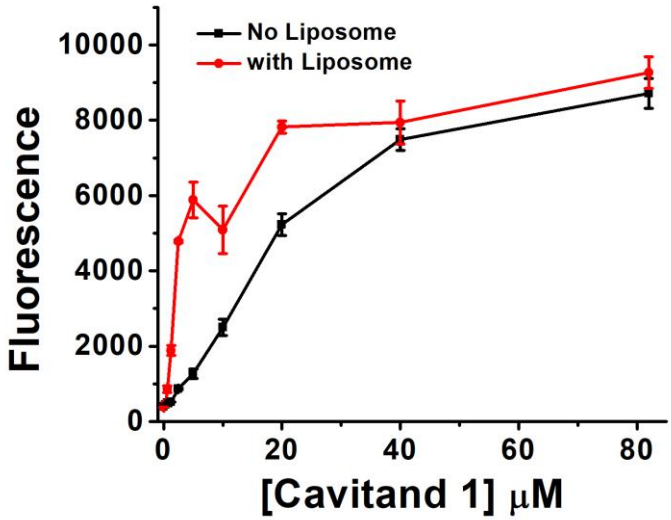

Figure S-6. Effect of liposome on the fluorescence of the **1•5** complex. [DSMI **5**] = 1.5 μM, liposome = 1 mg/mL, in 20 mM Tris at pH =7.4.

2. Linear Discriminant Analysis and Metal Sensing Data

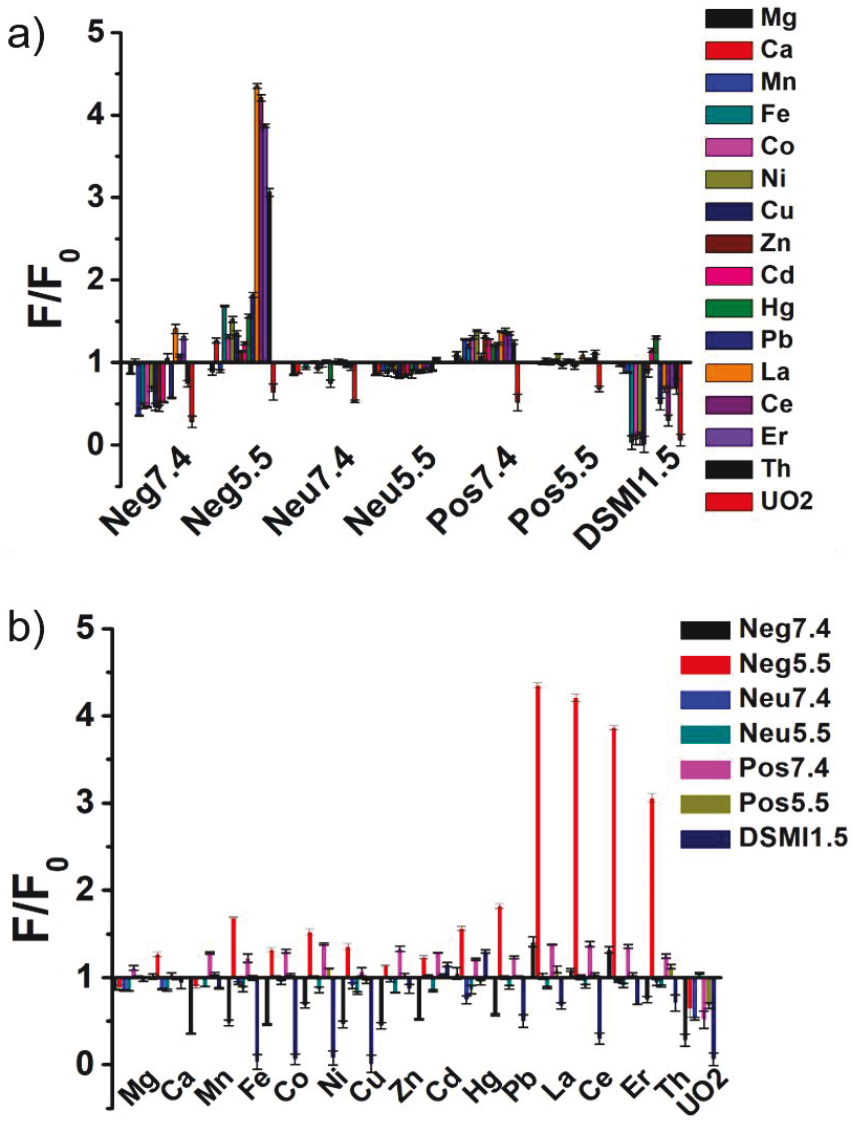

Figure S-7. The fluorescence data used for LDA to obtain the score plot shown in Figure 5c. a) Fluorescence plotted by array elements. b) Fluorescence plotted by metals. [Metal] = 50 μM, 20 mM Tris at pH 7.4 or 20 mM Bis-Tris at pH 5.5, [cavitand] = 4 μM for **1•4**, 20 μM for **1•5**, or 5 μM for **2•4** and **3•4**, [guest **4**] = 3 μM and [DSMI **5**] = 1.5 μM.

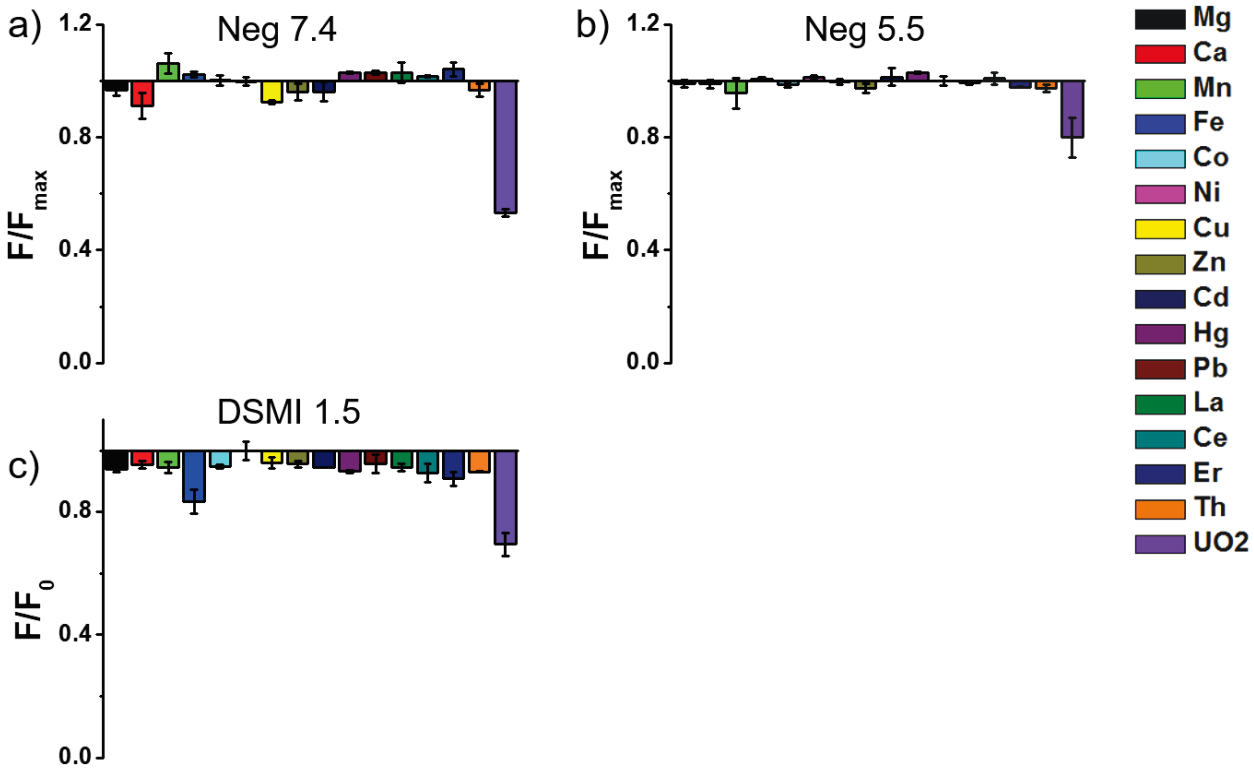

Figure S-8. Effect of metal salts on the emission intensity of a) guest **4** in Tris buffer (pH =7.4, 20 mM); b) guest **4** in Bs-Tris buffer (pH = 5.5, 20 mM); and c) DSMI **5** in Tris buffer (pH =7.4, 20 mM). All metals other than UO_2^{2+} and Fe^{2+} show negligible effects on both guests. [Metal] = 50 μM.

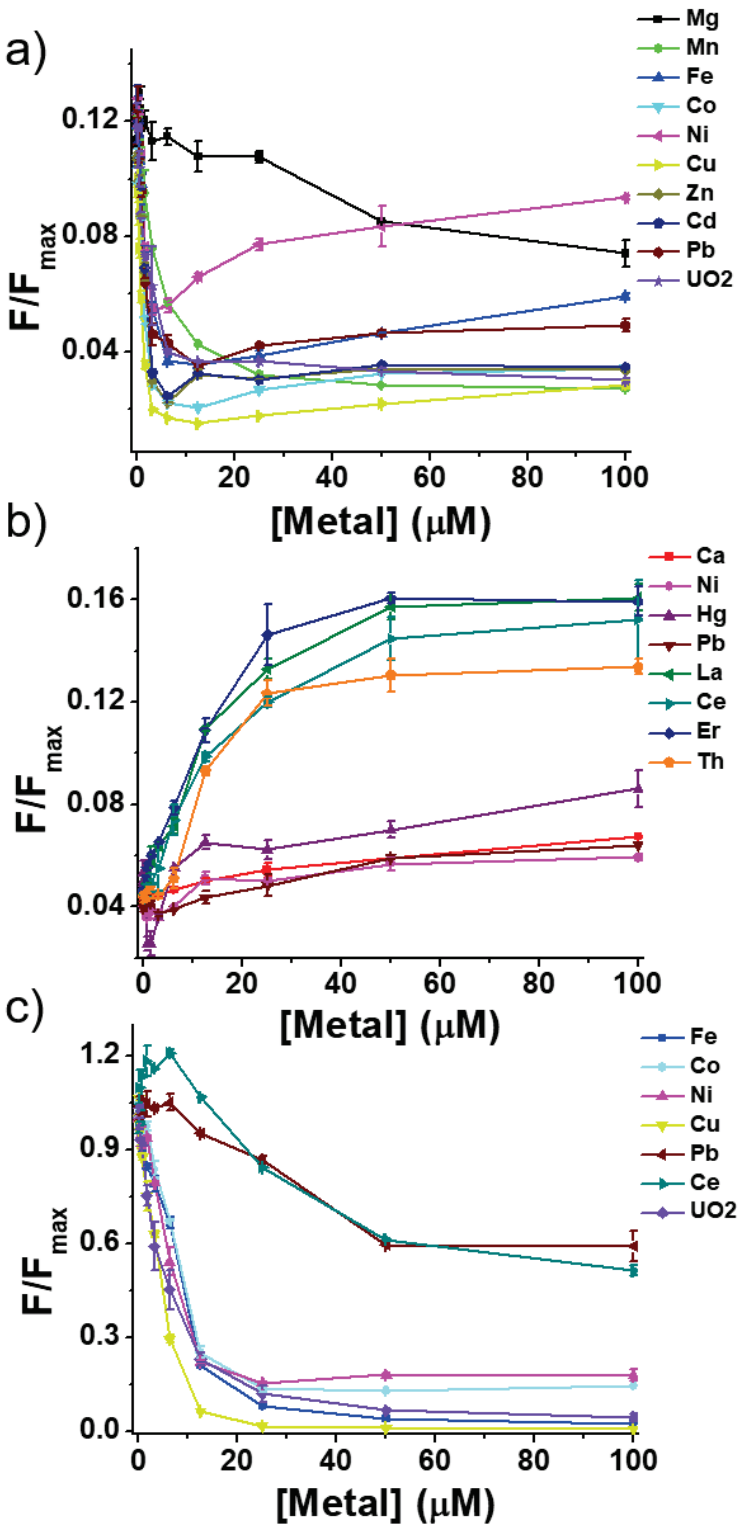

Figure S-9. The calibration curves showing change in sensor fluorescence upon addition of increasing [Metal] for the three sensors a) **1•4** at pH 7.4, b) **1•4** at pH 5.5 and c) **1•5** at pH 7.4. For **1•4**, [**1**] = 4 μM, [**4**] = 3 μM; for **1•5**, [**1**] = 20 μM, [**5**] = 1.5 μM.

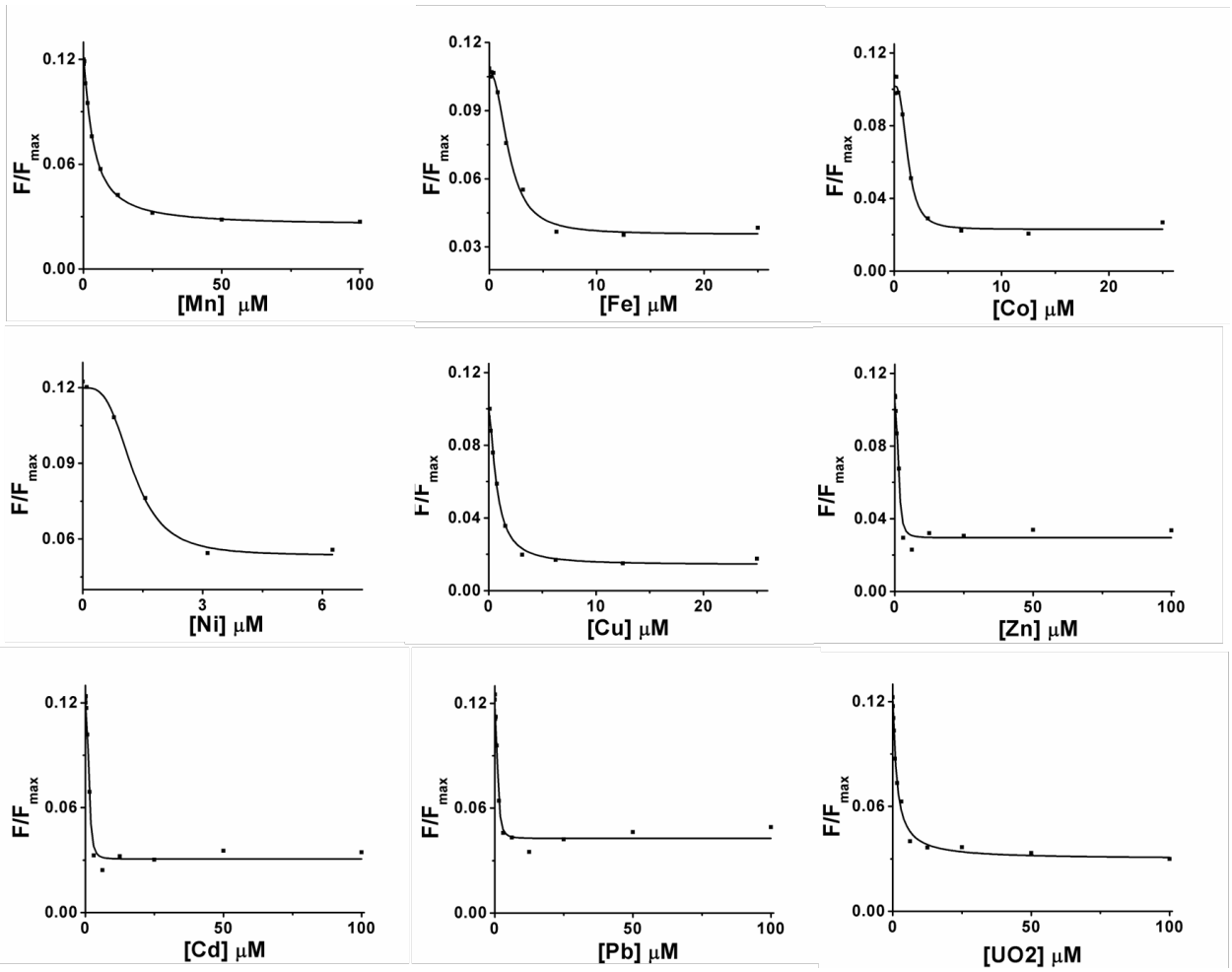

Figure S-10. The Hill plots for metals with complex **1•4** at pH 7.4.

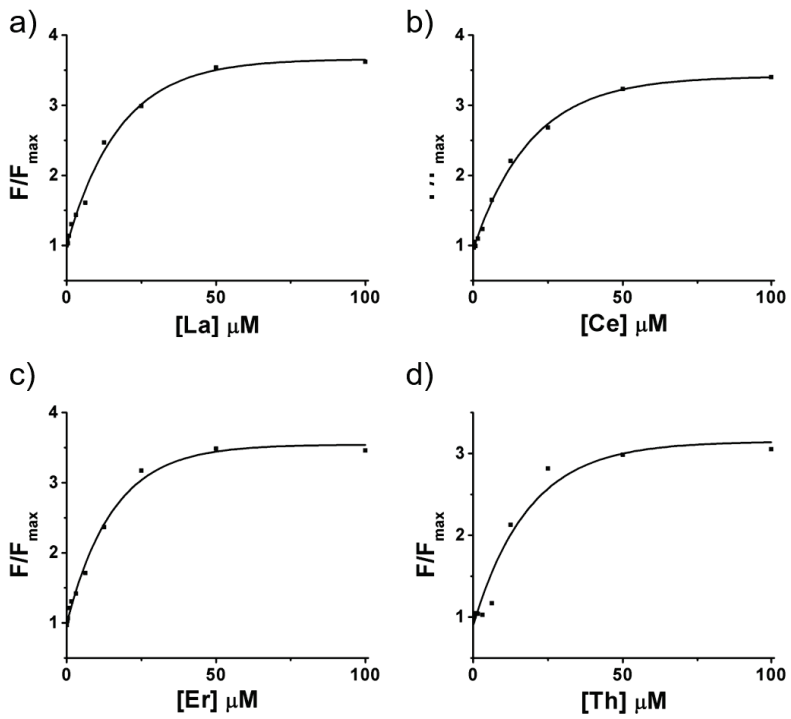

Figure S-11. The exponential fitting curves for calculation of IC_{50} in the metal displacement model for sensor **1•4** at pH 5.5 for the sensing of a) La^{3+}; b) Ce^{3+}; c) Er^{3+}; d) Th^{4+} salts.

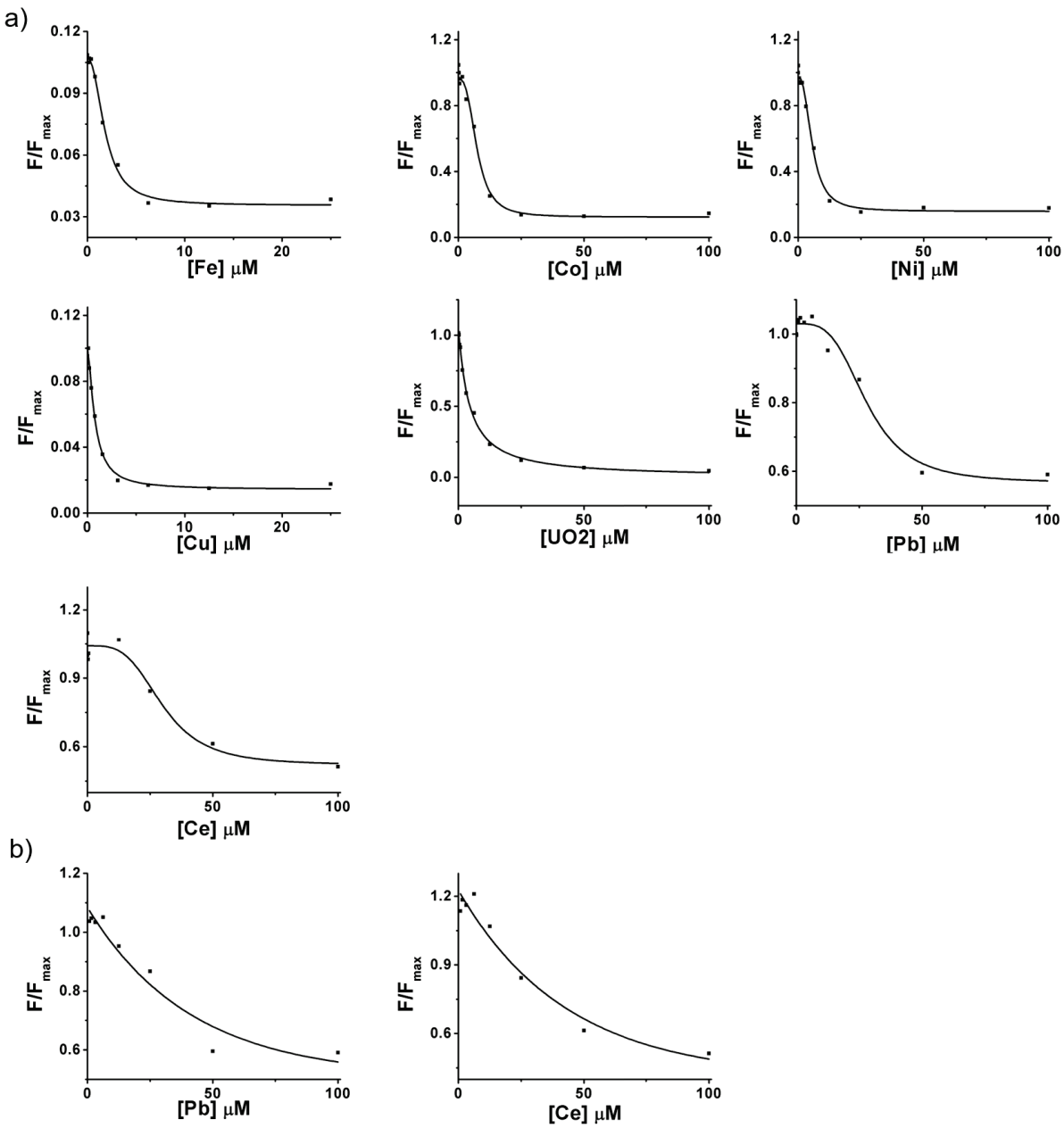

Figure S-12. a) Hill plot for the binding of Fe^{2+}, Co^{2+}, Ni^{2+}, Cu^{2+}, UO_2^{2+}, Pb^{2+} and Ce^{3+} to sensor **1•5** at pH 7.4, and b) exponential fitting for Pb^{2+} and Ce^{3+} for displacing **5** off cavitand **1** at pH 7.4.

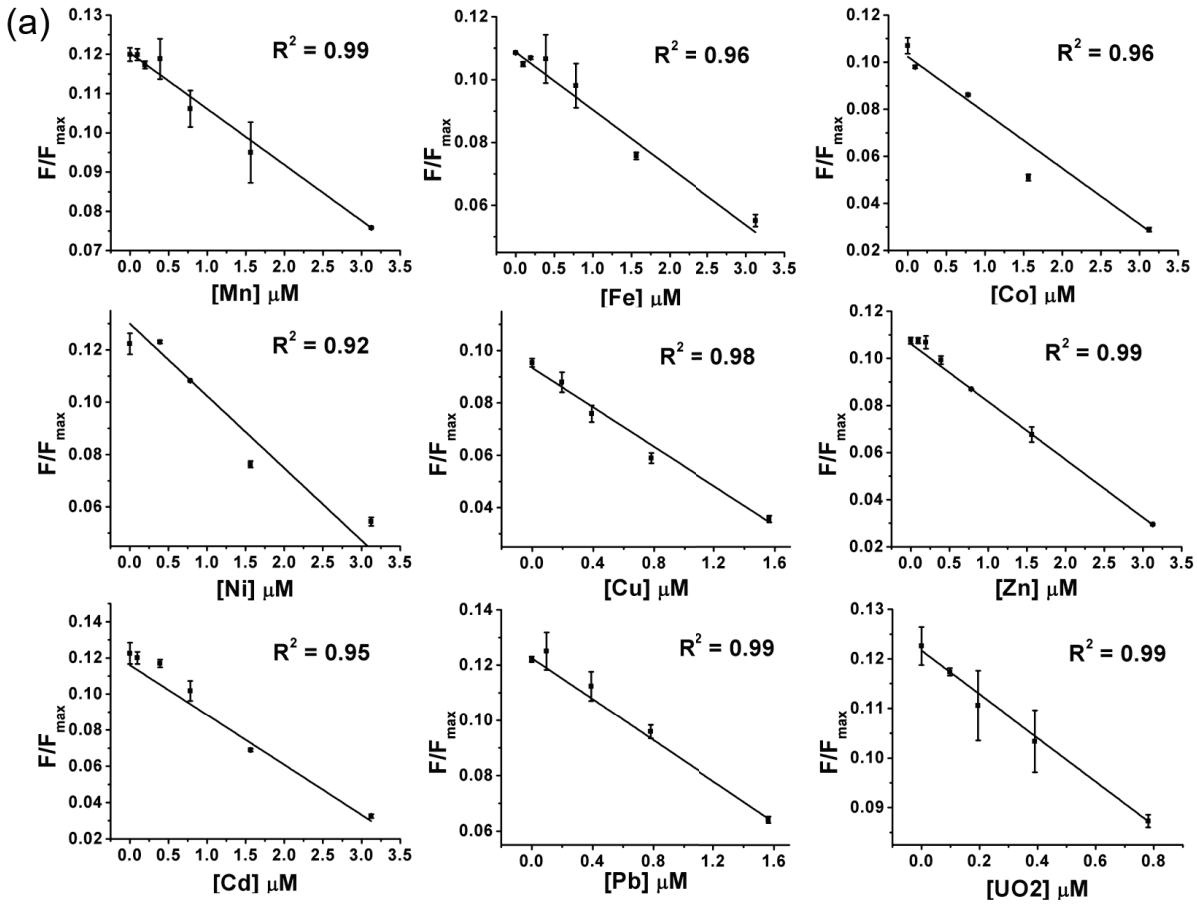
(a)
R² = 0.99
F/F max
[Mn] μM
R² = 0.96
[Fe] μM
R² = 0.96
[Co] μM
R² = 0.92
[Ni] μM
R² = 0.98
[Cu] μM
R² = 0.99
[Zn] μM
R² = 0.95
[Cd] μM
R² = 0.99
[Pb] μM
R² = 0.99
[UO2] μM

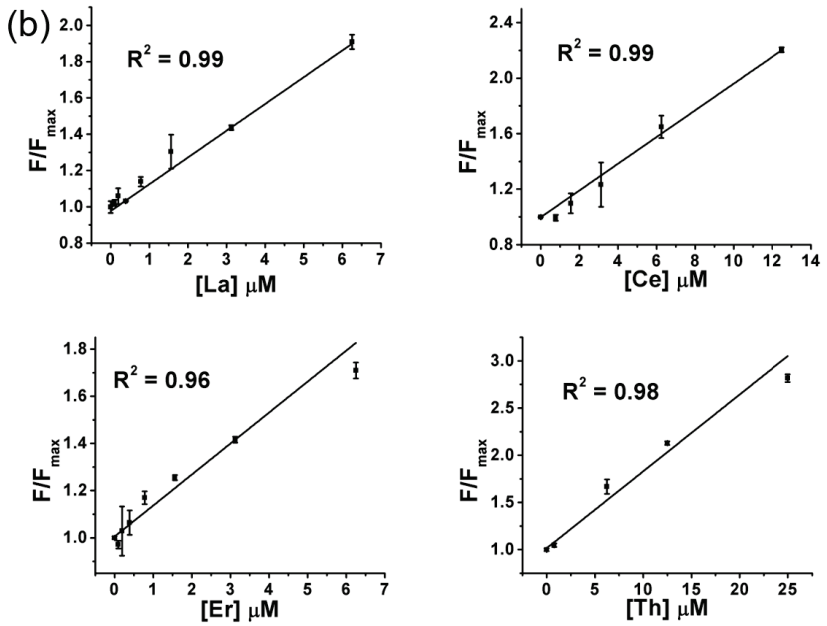
(b)
R² = 0.99
F/F max
[La] μM
R² = 0.99
[Ce] μM
R² = 0.96
[Er] μM
R² = 0.98
[Th] μM

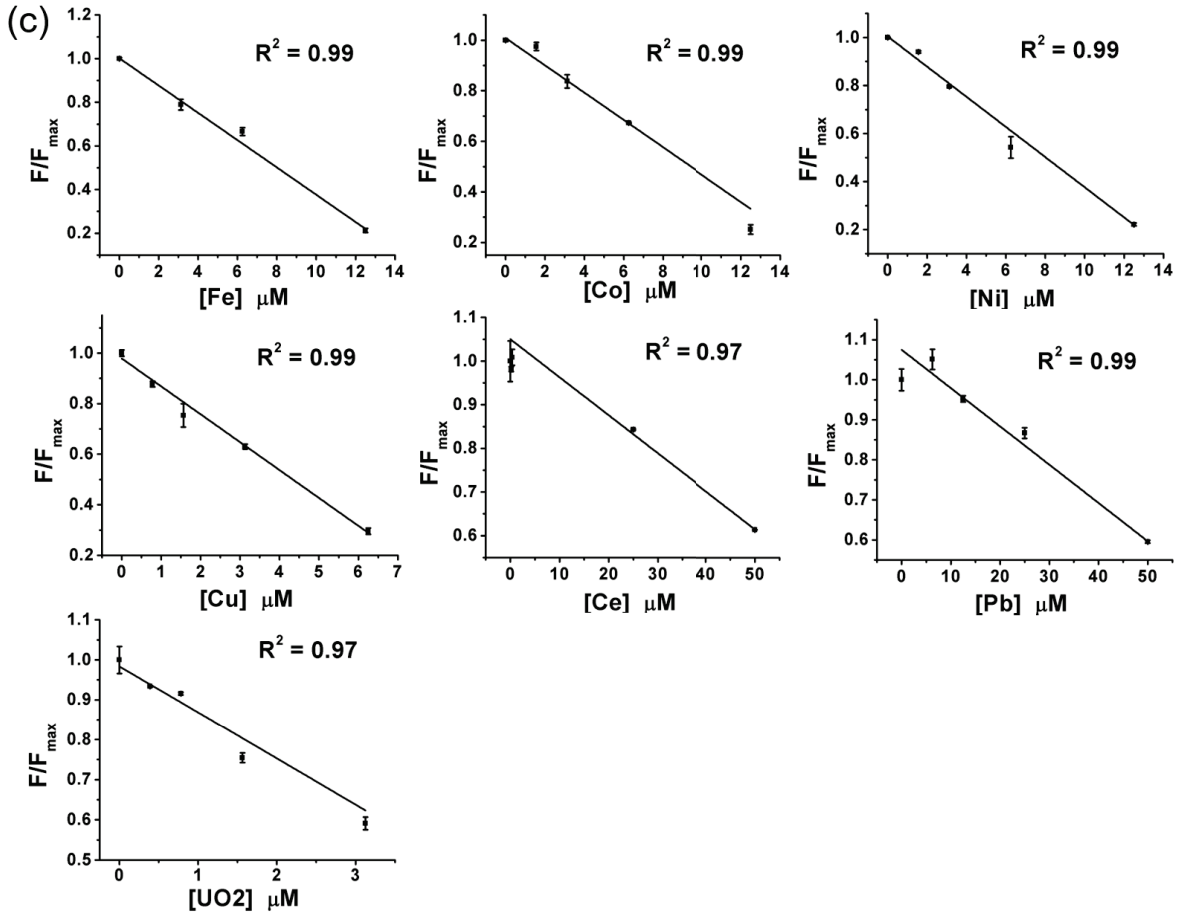

Figure S-13. Linear range for metal detection and LOD calculation. a) **1•4** at pH 7.4; b) **1•4** at pH 5.5; c) **1•5** at pH 7.4.

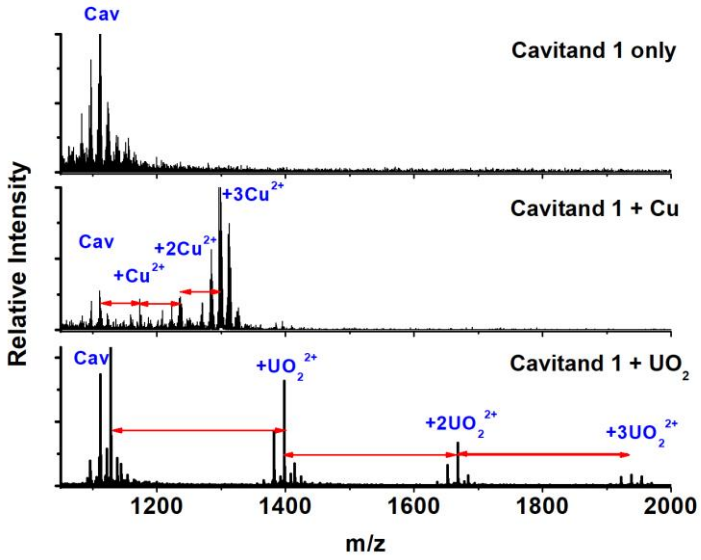

Figure S-14. SELDI-TOF-MS data for cavitand **1** binding Cu^{2+} and UO_2^{2+}. Other metals were tested as well but no complex ion was detected in gas phase, neither the cavitand-guest complex was detected.

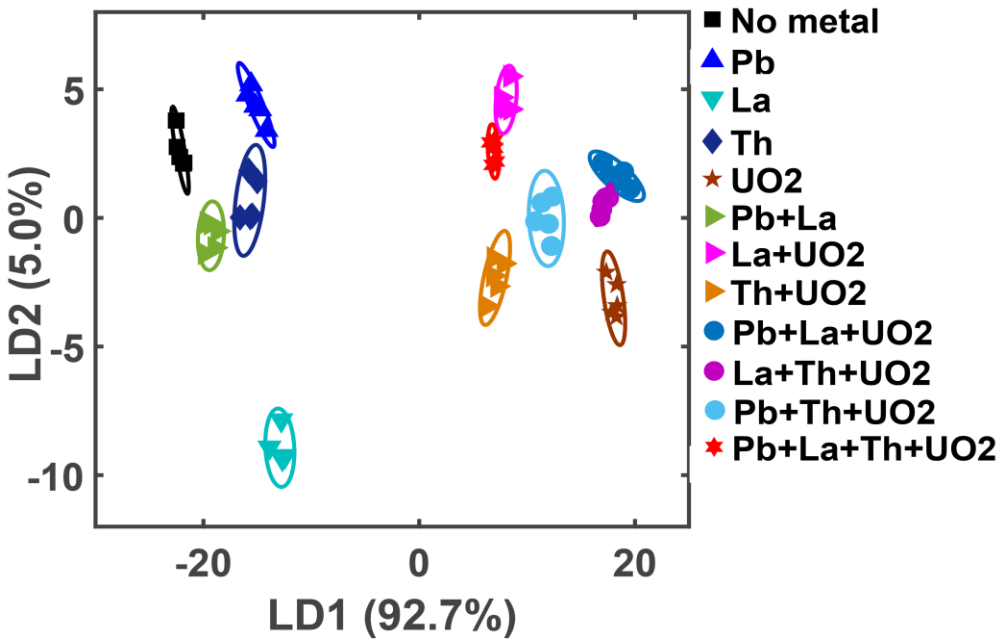

Figure S-15. LDA score plot for metal mixtures spiked in tap water with the three-factor sensor array containing **1•4** ([**1**] = 4 μM, [**4**] = 3 μM) in pH 7.4 or pH 5.5 buffer, and sensor **1•5** ([**1**] = 20 μM, [**5**] = 1.5 μM, pH 7.4). [Metal] = 2 μM, pH 7.4 = 20 mM Tris, pH 5.5 = 20 mM Bis-Tris.

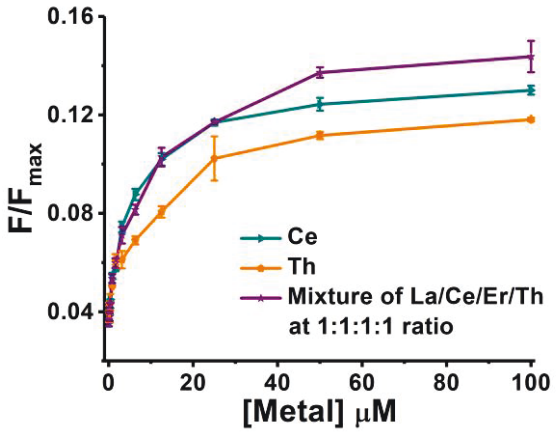

Metal	LOQ (μM)
Ce	1.26
Th	1.93
Metal Mixture (Ce,Th,La,Er)	2.12

Figure S-16. Titration curves for detection of metals in lake water (collected from the Lake Evans, Riverside), using the **1•4** sensor ([**1**] = 4 μM, [**4**] = 3 μM) at pH 5.5. The limit of quantitation (LOQ) was calculated using the 10σ method, and the lanthanides and actinides showed similar LOQ. This indicates that a single sensor allows metal detection with low LOQ, but not metal identification. However, with the full sensor array, we can provide semi-quantitative identification (see Table 3, main text).

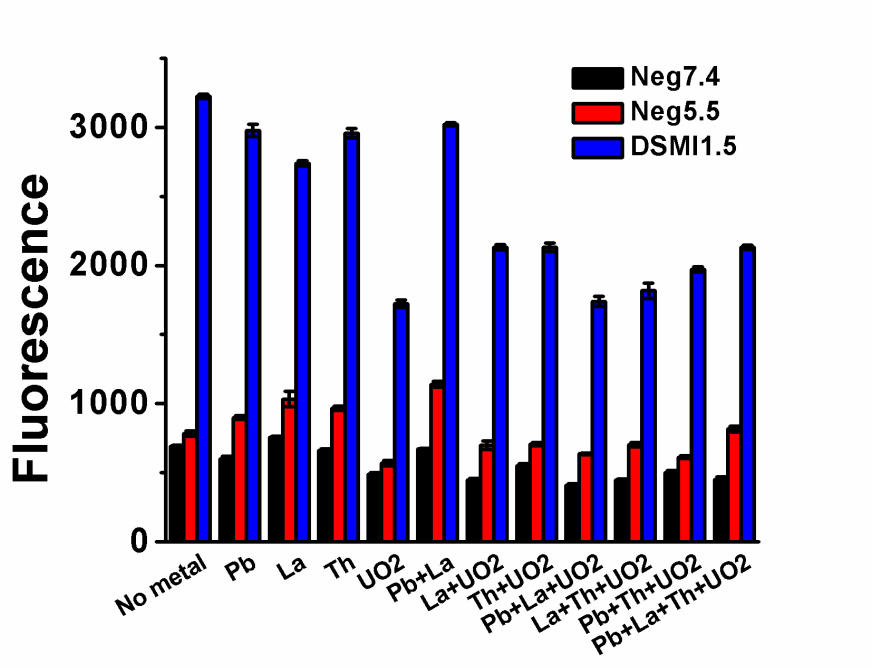

Figure S-17. The fluorescence data used for LDA to obtain the score plot shown in Figure S-15. [Metal] = 2 μM, 20 mM Tris at pH 7.4 or 20 mM Bis-Tris at pH 5.5, [cavitand **1**] = 4 μM and [guest **4**] = 3 μM for **1•4**, [cavitand **1**] = 20 μM and [DSMI **5**] = 1.5 μM for **1•5**.

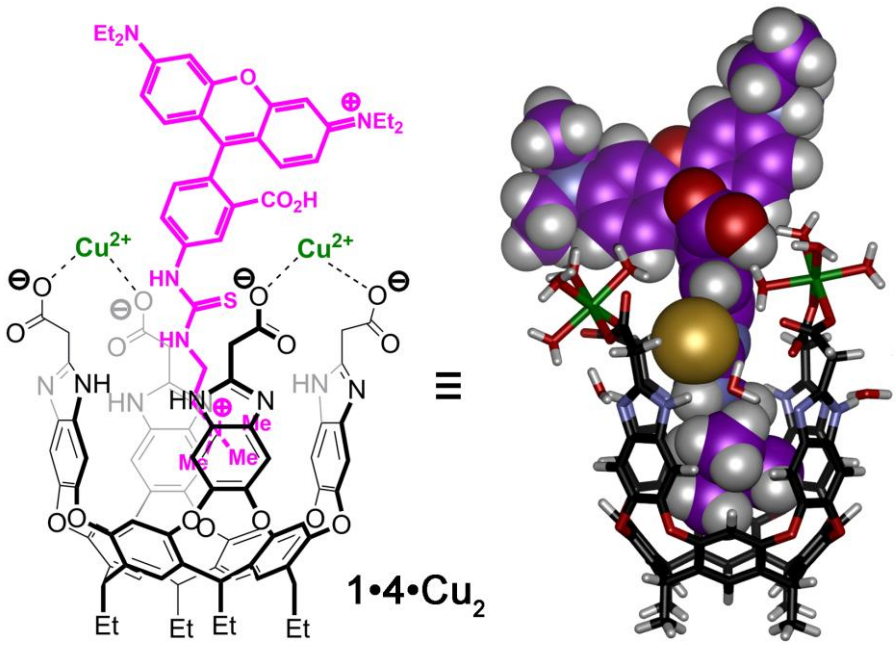

Figure S-18. Minimized structure of a) **1•4•Cu$_2$**, indicating the effect on metal orientation in the presence of a large guest (SPARTAN, AM1 forcefield).

Table S-1. Jackknife analysis of the fluorescence data shown in Figure 6a.

	Cd	Pb	Ce	La	Er	Hg	Th	UO2	%Correct
Cd	16	0	0	0	0	0	0	0	100
Pb	0	16	0	0	0	0	0	0	100
Ce	0	0	16	0	0	0	0	0	100
La	0	0	0	16	0	0	0	0	100
Er	0	0	0	0	16	0	0	0	100
Hg	0	0	0	0	0	16	0	0	100
Th	0	0	0	0	0	0	16	0	100
UO2	0	0	0	0	0	0	0	16	100
Total	16	16	16	16	16	16	16	16	100

Table S-2. Jackknife analysis of the fluorescence data shown in Figure S16, agreeing with the score plots shown in Figure 7.

	No metal	Pb	La	Th	UO2	La+UO2	Th+UO2	Pb+La+ UO2	La+Th +UO2	Pb+La+ Th+UO2	%Correct
No metal	5	0	0	0	0	0	0	0	0	0	100
Pb	0	5	0	0	0	0	0	0	0	0	100
La	0	0	5	0	0	0	0	0	0	0	100
Th	0	0	0	5	0	0	0	0	0	0	100
UO2	0	0	0	0	5	0	0	0	0	0	100
Pb+La	0	0	0	0	0	0	0	0	0	0	100
La+UO2	0	0	0	0	0	5	0	0	0	0	100
Th+UO2	0	0	0	0	0	0	5	0	0	0	100
Pb+La+UO2	0	0	0	0	0	0	0	5	0	0	100
La+Th+UO2	0	0	0	0	0	0	0	0	5	0	100
Pb+Th+UO2	0	0	0	0	0	0	0	0	0	0	100
Pb+La+Th+UO2	0	0	0	0	0	0	0	0	0	5	100
Total	5	5	5	5	5	5	5	5	5	5	100

Table S-3. Dissociation constants obtained from curve fitting and limit of detection (LOD) calculated for all metals tested in Figure S10.

Sensor	Metal	K_d^{MC} (μM) by Hill plot	n by Hill plot	LOD (μM)
1•4 At pH 7.4	Mn^{2+}	4.5±0.3	1.2	0.51
	Fe^{2+}	3.8±1.4	2.1	0.23
	Co^{2+}	2.0±0.4	2.7	0.22
	Ni^{2+}	1.8±0.4	3.1	0.48
	Cu^{2+}	0.7±0.1	1.4	0.07
	Zn^{2+}	2.7±0.8	2.0	0.22
	Cd^{2+}	2.5±0.3	2.3	0.52
	Pb^{2+}	1.3±0.3	2.0	0.13
	UO_2^{2+}	1.4±0.2	1.1	0.23

Sensor	Metal	IC50 (μM) by Displacement Model	R^2	K_d^{D} (μM) by Displacement Model	LOD (μM)
1•4 At pH 5.5	La^{3+}	12.27	0.99	1±0.1	0.58
	Ce^{3+}	13.43	0.99	1.1±0.1	1.21
	Er^{3+}	10.74	0.99	0.9±0.1	0.31
	Th^{3+}	12.75	0.95	1.1±0.1	1.29

Sensor	Metal	K_d^{MC} (μM) by Hill plot	n by Hill plot	IC50 (μM) by Displacement Model	R^2	K_d^{D} (μM) by Displacement Model	LOD (μM)
1•5 At pH 7.4	Fe^{2+}	58±14	2.0	7.07	0.98	NA	0.19
	Co^{2+}	200±40	2.6	6.71	0.97	NA	0.51
	Ni^{2+}	73±14	2.5	5.19	0.98	NA	0.33
	Cu^{2+}	8.7±1.7	1.6	3.71	0.99	NA	0.21
	Ce^{3+}	(1.9 ±0.6) x 10^3	2.3	17.92	0.99	2.7±0.1	4.60
	Pb^{2+}	(1.3±0.3) x 10^3	1.5	35.78	0.97	12.2±1.7	9.15
	UO_2^{2+}	4.9±0.5	1.1	4.35	0.99	NA	0.27

4. References

1. de la Peña, A. M.; Salanas, F.; Gómez, M. J.; Acedo, M. I.; Peña, M. S. *J. Inclus. Phenom. Mol. Rec. Chem*. **1993**, *15*, 131-143.